Food Chemistry: X 26 (2025) 102290

Contents lists available at ScienceDirect

Food Chemistry: X

journal homepage: www.sciencedirect.com/journal/food-chemistry-x

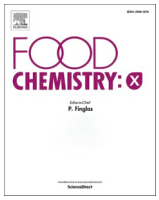

Characteristics of exopolysaccharides - egg white protein composite gel and its application in low - fat sausage

Guoguo Jin, Man Zhang [1], Xinran Wang, Yifan Zhang, Guohua Jiang, Lin Mei [*]

College of Food and Nutrition, Anhui Agricultural University,130 Changjiang West Road, Hefei, 230036, Anhui, PR China

ARTICLE INFO

Keywords:
Fat substitute
Exopolysaccharides - egg white protein composite gels
Molecular docking analysis

ABSTRACT

A composite gel was developed by integrating antioxidant extracellular polysaccharides (EPS) derived from *Pediococcus acidilactici* S1 with egg white protein (EWP), aiming to evaluate its potential as a viable alternative to animal fat in pork sausages. The results indicated that the EPS - EWP gel exhibited a lower free water content, an enhanced water - holding capacity, a higher apparent viscosity, and increased storage and loss modulus. Molecular interactions were strengthened, resulting in a more stable structure characterized by the transition of secondary structure from random coils to ordered β - sheets. Molecular docking (MD) analysis revealed favorable binding conformations and strong binding energies between ovalbumin (OVA) and EPS, particularly through the formation of specific pockets involving interactions with residues such as Lysine (Lys) and Aspartic acid (Asp). Hydrophobic and electrostatic forces were identified as the primary driving forces for this energetic combination. Additionally, low - fat sausages showed a significant 32.87 % improvement in inhibiting fat oxidation.

1. Introduction

Fat in meat products is favored by consumers for its nutritional content and sensory properties. However, traditional meat products contain large amounts of saturated fatty acids and cholesterol, which can pose potential health risks if consumed in excess (Yu et al., 2023). Fat substitutes are an effective way to address the health issues related to high-fat meat products (Josquin et al., 2011; Saygi et al., 2018). However, substitutes may lead to problems such as deteriorated taste and texture, and shortened shelf life. Food hydrocolloids are another type of fat substitute and can be classified into protein-based and polysaccharide - based fat substitutes. Polysaccharide - based fat substitutes are safer, more widely available, and lower in calories, and have been extensively studied in recent years (Yang et al., 2020).

However, single protein and polysaccharide fat mimetics do not simultaneously possess all these ideal characteristics. Using protein alone or polysaccharides alone has various functional and sensory limitations, such as poor mouthfeel and stability issues concerning salt, pH, heat treatment, and freeze - thaw cycles (Guo et al., 2018). Therefore, to mimic the functional quality of fat, combinations of two or more fat mimetics have been synergistically utilized. Yang et al. (2023) prepared conjugates of casein (CA) with pectin (CP) or arabinogalactan (AG) via the Maillard reaction under wet heating. They found that compared with CA alone, CA - CP and CA - AG conjugates exhibited lower surface hydrophobicity and higher absolute ζ - potential values. Protein - polysaccharide-based fat substitutes have been used to replace fat in foods, thus producing low - fat foods. Due to their interactions, these complexes have been shown to possess better functionality than using each component alone. Proteins and polysaccharides have a wide range of physicochemical properties that can be used to determine various complex system properties when mixed, such as increased protein solubility, enhanced foam stability, and stabilized emulsion - based systems. Due to the high molecular weight and numerous functional groups of these biopolymers, they can also effectively interact with water and other molecules, thereby promoting system stability (Hoff et al., 2000) (Fig. 1).

Exopolysaccharides (EPS) produced by lactic acid bacteria (LAB) are considered safe (Kumar et al., 2007). In the field of food science, a groundbreaking natural additive has attracted significant academic attention due to its unique physiological effects and enormous potential, opening up new research areas. Based on the composition of monomers, EPS can be divided into homopolysaccharides (HoPS) and heteropolysaccharides (HePS), therefore their structures are more complex and diverse. EPS is of great interest due to its complex biological activities,

* Corresponding author.
E-mail address: meilin@ahau.edu.cn (L. Mei).
[1] Co - first author.

https://doi.org/10.1016/j.fochx.2025.102290
Received 26 December 2024; Received in revised form 13 February 2025; Accepted 16 February 2025
Available online 19 February 2025

including antioxidant, anti-tumor, maintaining tissue cell integrity, lowering cholesterol, and regulating the immune system (Elnahas et al., 2017; Zhou et al., 2018). Currently, the utilization rate of LAB EPS in the food industry is significantly lower than that of plant and animal polysaccharides due to its limited yield, which restricts large-scale industrial application. However, when added in situ without compromising the overall texture of the product, the EPS produced by LAB in situ is more in line with consumers' demand for fewer additives in food (Zhang et al., 2024). Therefore, LAB that produce EPS play an increasingly important role in the food industry. In the food production, LAB EPS plays the role of gelling agent, emulsifiers, stabilizer and thickener through special structure. LAB EPS can change the texture, sense, flavor and taste of food by affecting rheology, hardness and viscosity, especially in the dairy products, plant-based yogurt beverages, cereal products and meat products. However, it must be acknowledged that research on the application of EPS in the meat industry, especially in the development of low-fat meat products, is still in its infancy (Loeffler et al., 2020).

Egg white (EW) contains about 13 % to 15 % total protein (Wilson, 2017). These components confer excellent gelling, emulsifying, foaming, and thickening properties to egg white protein (EWP) (Xia et al., 2022). In addition, EWP also has antioxidant, antibacterial, antiviral, and immunomodulatory activities closely related to human health (Sun, Jin, et al., 2020). As a functional food ingredient, gelling properties are one of the key functions of EWP, often playing a crucial role in surimi and meat products. The gelation performance of proteins in minced meat products is a key factor affecting the basic functional properties of the product. Protein gelation provides unique mouthfeel and texture to protein foods. During gelation, covalent and non-covalent interactions between protein molecules randomly form an extensive network structure (Rombouts et al., 2020), capturing more water molecules and water - soluble elements, thus giving the product a juicy and richer flavor (Xia et al., 2022).

This study aims to innovate in the field of natural and safe food ingredients by focusing on the development and application of functional microbial polysaccharides in new forms of hydrocolloids. By utilizing the excellent properties of composite gels, this research provides a new perspective on the use of fat substitutes, which are essential for producing low - fat and functional foods. The incorporation of these composite gel systems not only aligns with the trend of healthy food development but also meets the evolving social norms and consumer expectations for healthier dietary choices.

2. Material and methods

2.1. Materials

Sterile chicken eggs and pork (hind leg meat and back fat) were purchased from the Carrefour Supermarket in Hefei; Man Rogosa Sharpe (MRS) broth medium was obtained from Hangzhou Base Biotechnology Co., Ltd.; anhydrous ethanol was supplied by Shanghai Zhenxing Chemical; trichloroacetic acid (AR, ≥ 99.0 %) and 2 - thiobarbituric acid (≥ 98 %) were acquired from Shanghai Macklin Biochemical Co., Ltd.; ethylenediaminetetraacetic acid (≥ 99.0 %), sodium hydroxide, sodium chloride, urea, and sodium tripolyphosphate were purchased from Sinopharm Chemical Reagent Co., Ltd.; protein quantitation (TP) assay kits (bicinchoninic acid method, Coomassie Brilliant Blue method) were sourced from Nanjing Jiancheng Bioengineering Institute; standard dialysis bags (MD1444, 8000–14,000 kDa) were provided by Shanghai Yuan Ye Biological Technology Co., Ltd.; *Pediococcus acidilactici* S1 was obtained from the Laboratory of Livestock Products Processing at Anhui Agricultural University and is preserved in the China General Microbiological Culture Collection Center (CCTCC) under the preservation number CCTCC NO: M2021229.

2.2. Extraction, separation, and purification of S1 - EPS

Pediococcus acidilactici S1 was inoculated into MRS broth at 37 °C for 24 h. This process was repeated twice, with each inoculation using 10 % of the previous culture. Subsequently, 2 % of this culture was inoculated into MRS broth. After fermenting at 37 °C for 16 h, the mixture was centrifuged at 10,000 rpm for 20 min at 4 °C. The supernatant, referred to as cell - free supernatant was collected (Lu et al., 2023). The supernatant was then heated in a boiling water bath for 5 min to inactivate the medium and hydrolytic enzymes, and subsequently cooled to room temperature (25 °C). Trichloroacetic acid (TCA) was added to the supernatant to achieve a final concentration of 12 %, and the mixture was thoroughly stirred. The solution was allowed to stand for 4–8 h to precipitate proteins and enzymes. Subsequently, the cell - free supernatant was subjected to another round of centrifugation in order to collect the supernatant. Anhydrous ethanol, three times the volume of the supernatant, was then added and the mixture was left at 4 °C for 12 h to induce flocculation. Finally, the resulting mixture was centrifuged at 15, 000 rpm for 30 min at 4 °C to obtain a precipitate which was subsequently dissolved in deionized water and placed in a dialysis bag (with a

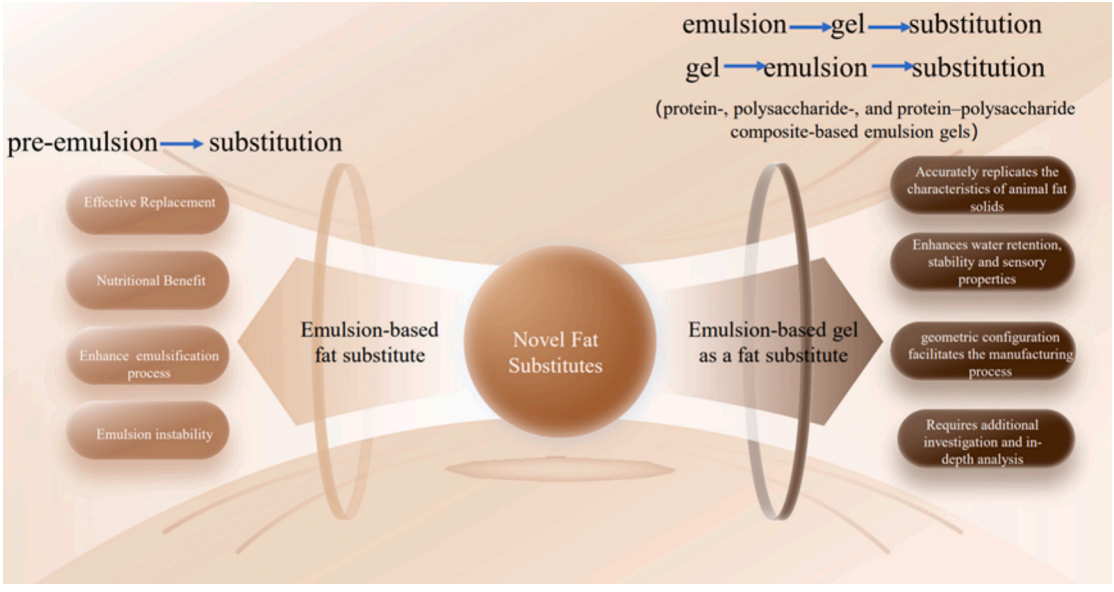

Fig. 1. The application of gels as fat substitutes.

molecular weight cutoff of 14, 000 Da) for 48 h with water changes every 12 h, yielding an extracellular polysaccharide solution. The crude extract obtained from this process was freeze - dried for 24 h in petri dishes to yield the crude polysaccharide.

The isolation and purification of crude polysaccharides were performed according to the methods of Lu et al. (2024). Initially, the dried crude polysaccharides were crushed and treated overnight with an ethanol solution for degreasing and decolorization. The dried residue was extracted by Sanli Biotechnology Co., Ltd. (Shanghai, China) using a 1: 10 material - to - water ratio (hot water) at 60 °C for 4 h. As described above, the precipitate was re - extracted twice, and the supernatants were pooled. The extract was concentrated and precipitated with 4 times its volume of anhydrous ethanol at 4 °C to obtain a crude aqueous extract. The dried crude aqueous extract was then dissolved in water, and proteins were removed using the Sevage method, lipids were removed using petroleum ether, and pigments were removed using macroporous resin AB - 8. The solution was dialyzed against water (3000 Da), concentrated, and lyophilized to obtain crude polysaccharides. The crude polysaccharides were applied to a DEAE - cellulose column (26 mm × 400 mm), eluted sequentially with distilled water at 4 mL/min, followed by 0.1 M, 0.2 M, and 0.3 M sodium chloride, and the fractions were collected. The carbohydrate content was determined by Sanli Biotechnology Co. at 490 nm using the phenol-sulfuric acid method. The major polysaccharide fractions were collected, concentrated, and dialyzed against distilled water (3000 Da) for 48–72 h. Subsequently, the polysaccharide solution was loaded onto a Sephacryl S - 400 HR column (26 mm × 1000 mm), eluted with distilled water at 1.0 mL/min, and monitored using the phenol-sulfuric acid method. The purified polysaccharides obtained by this method referred to as EPS, had a total sugar content of up to 94.8 %.

2.3. Preparation of SI EPS - egg white protein (EPS - EWP) composite gels

Gels were prepared according to the method described by Zhang et al. (2023). The fresh egg whites were separated and dispersed using a high - speed homogenizer at 3000 rpm for 6 min to obtain a natural and uniform liquid form of egg white, which was subsequently lyophilized into powder form and stored at 4 °C under sealed conditions.

The lyophilized egg white powder was dissolved in deionized water to prepare an 8 % solution of EWP. While stirring, varying concentrations (0 %, 2 %, 4 %, 6 %, and 8 %) of EPS (*w/v*, based on the volume of the egg white protein solution) were added to the aforementioned solution. The pH was adjusted to 8.0 using citric acid. Subsequently, the mixture of EPS - EWP was heated in a water bath at 90 °C for a duration of 30 min to induce gel formation. Immediately after heating, the mixture was rapidly cooled in an ice water bath. Finally, the beaker containing the samples was tightly covered with plastic wrap and stored at 4 °C for a period of 12 h prior to testing their gel properties.

2.4. Texture profile analysis (TPA)

Samples were brought to room temperature (25 °C) and cut into cylinders of 10 mm × 30 mm (height × diameter). Texture Profile Analysis (TPA) was then performed using a P/50 probe on a texture analyzer, following the method described by Ma et al. (2021), to determine the hardness and elasticity of the gel or sausage samples. The test parameters were as follows: pre-test speed: 2.0 mm/s; test speed: 1.0 mm/s; post - test speed: 1.0 mm/s; distance: 5 mm; trigger force: 5 g. Each sample was tested six times ($n = 6$).

2.5. Color difference measurement

The color parameters of the samples, including lightness (L*), redness (a*), and yellowness (b*), were measured using a CR - 400 handheld colorimeter according to the method described by Weng and Zheng (2015). A white standard plate (L* = 92.75, a* = − 0.48, b* = 5.55) was used as the reference. The colorimeter was placed on the surface of the sample to record the values, and each test was repeated three times. The total chromatic difference (ΔE) of the protein samples was calculated by the following formula.

$$\Delta E = \sqrt{(L_0^* - L^*)^2 + (a_0^* - a^*)^2 + (b_0^* - b^*)^2}$$

where L_0*, a_0*, and b_0* represent the color parameters of the blank sample.

2.6. Water holding capacity (WHC) analysis

Following the method described by Mirarab Razi et al. (2018), the water holding capacity (WHC) of gel samples was determined. The mass of an empty centrifuge tube was weighed and recorded as m_0. The 15 g of the sample was placed into the centrifuge tube, and the total mass of the gel and tube before centrifugation was recorded as m_1. The sample was then centrifuged at 6000 rpm for 20 min. After centrifugation, the tube was inverted on absorbent paper, and the expelled water was removed using filter paper. The total mass of the gel and tube after centrifugation was weighed and recorded as m_2. The WHC of the sample was calculated using the following formula, with each sample measured in triplicate and the average value taken.

$$\text{WHC}\ (\%) = \frac{m_2 - m_0}{m_1 - m_0} \times 100$$

2.7. Scanning electron microscopy (SEM) analysis

The microstructure of the samples was observed using the method described by Xue et al. (2021). Freeze - dried samples of the EPS - EWP gels were sliced with a blade and mounted on an SEM column using double-sided conductive tape, followed by gold sputtering using a Model IB - 3 Ion Sputter. The samples were then placed in a scanning electron microscope (Hitachi S - 4800, Japan) and observed at an acceleration voltage of 3 kV with a magnification of 4000 times, using XT Microscope Control software to capture the images.

2.8. Determination of intermolecular forces

Using the method described by Wu et al. (2021) with minor modifications, the intermolecular forces of the composite gels were measured. Gel samples (1 g each) were mixed with solution S_1 (0.6 M NaCl) and homogenized for 1 min. The homogenate was then allowed to stand at 4 °C for 1 h, and the supernatant was collected. The resulting precipitate was mixed with solution S_2 (1.5 M urea +0.6 M NaCl), homogenized, and then centrifuged at 10,000 r/min for 10 min at 4 °C, with the supernatant again collected. The precipitate obtained was sequentially mixed with solution S_3 (8 M urea +0.6 M NaCl) and solution S_4 (0.5 M β - mercaptoethanol +0.6 M NaCl +8 M urea), homogenized, centrifuged, and all resulting supernatants were collected. Finally, the protein content in the supernatants was measured using a total protein (TP) assay kit. Each sample was tested three times. The solubility in S_1, S_2, S_3, and S_4 respectively represents the contribution of ionic bonds, hydrogen bonds, hydrophobic interactions, and disulfide bonds.

2.9. Molecular docking simulation between EPS and EWP

Following the method by Fu et al. (2020) with modifications, the AutoDock software was used to simulate docking of the main protein, ovalbumin, in EWP with EPS, analyzing their binding sites and predicting the intermolecular forces between ovalbumin and EPS molecules through https://plip-tool.biotec.tu-dresden.de/plip-web/plip/index. The three-dimensional structure of ovalbumin was obtained from the RCSB PDB database (http://www.rcsb.org/) at https://doi.org/

10.2210/pdb1JTI/pdb, and the three-dimensional structure of EPS was sourced from the PubChem database (https://pubchem.ncbi.nlm.nih.gov/). After removing water and substrates, polar hydrogen atoms were added to the receptor, and the protein crystal structure was prepared using Auto Dock software. The docking simulation was performed using Auto Dock Vina1.2.2 software. A grid box covering the entire binding site was created with centers at X: 92.05, Y: 92.05, and Z: 92.05. Ten docking trials were conducted to select the best binding mode, and the interactions between the ligand and the active site of the receptor were illustrated using PyMol software.

2.10. Molecular dynamics simulation of EPS and EWP

The stability and conformation of the thermally induced EPS - EWP composite gel were studied using molecular dynamics (MD) simulation. The MD simulations of the protein-ligand (ovalbumin - EPS) complex, obtained through molecular docking, were performed using Gromacs2020 software (Adachi et al., 2001; Yoshizawa et al., 2011). The two systems were conveniently constructed using CHARMM - GUI (Jo et al., 2008). The protein and ligand models were constructed and optimized using the CHARMM and CGenFF force fields, respectively (Best et al., 2012; Klauda et al., 2010). The system was solvated using the TIP3 water model and neutralized with potassium and chloride ions. Before production simulations, the system was minimized for 100 ps using the steepest descent algorithm to eliminate any unnatural clashes. Subsequently, a 250 ps equilibration process was conducted, gradually releasing scaled restraints until the forces were completely removed. MD simulations were performed under NPT conditions at a temperature of 303.15 K and a pressure of 1 atm, with a time step of 2 fs, using the LINCS algorithm to constrain bonds involving hydrogen atoms. The Particle Mesh Ewald (PME) method was used to calculate electrostatic interactions (Yong et al., 2021). All simulations were conducted using the Gromacs 2021.6 software package (Abraham et al., 2015). Conformational superposition and motion trends were plotted using Pymol (Yuan et al., 2017).

2.11. Rheological properties analysis

Following the method described by Bi et al. (2016), the apparent viscosity of different samples were measured at room temperature (25 °C) after restoring the samples to room temperature. The parameters for measurement included a parallel plate diameter of 40 mm, a gap of 1 mm, and a shear rate range of 0.01–100 s^{-1}. Each sample was measured in triplicate, and the results were averaged. According to the method by Razi et al. (2018), prepared samples were subjected to a frequency sweep experiment using oscillation mode. The specific parameters included a strain of 1 %, and the storage modulus (G'), loss modulus (G"), and loss factor (tan δ = G"/G') were measured at 25 °C across a frequency range of 0.1 to 25 Hz in order to ascertain their frequency-dependent variations.

2.12. Low-field nuclear magnetic resonance (LF - NMR)

Following the method described by Zhao et al. (2023), nuclear magnetic resonance imaging was employed to measure the transverse relaxation time (T_2) of samples, analyzing the moisture migration in composite gels or sausage samples. Samples loaded in 2 mL vials were placed in NMR tubes with a diameter of 15 mm at the center of the RF coil. The CPMG sequence was used for sample measurement. The parameters were set as follows: repetition sampling interval: TW = 1000.0 ms, number of accumulative scans: NS = 16, echo time: TE = 0.3 ms, number of echoes: NECH = 8000. After sampling, the Numaris NMR inversion software was used to invert the obtained CPMG exponential decay curve, producing a low - field nuclear magnetic relaxation time spectrum. From this, the transverse relaxation time (T_2) of the samples were obtained, and the relaxation peaks were integrated to obtain the peak area (A_2), with each sample measured in triplicate.

2.13. Fourier transform infrared spectrometer (FTIR)

According to the method described by Shi et al. (2022), the secondary structural changes in the proteins of the samples were analyzed using the FTIR. The lyophilized samples (1 mg) were mixed with potassium bromide (100 mg). The mixture was then ground into a uniform powder and pressed into thin discs. The protein secondary structures of the samples were determined using an FTIR spectrometer (IS10, Thermo Nicolet Instruments, USA). The wavenumber range was from 4000 cm^{-1} to 500 cm^{-1}, with a resolution of 4 cm^{-1} and 64 scans at an ambient temperature of 25 °C. The spectral data were analyzed using OMNICV8.0 software, and the transmittance at the wavenumber range of 1600–1700 cm^{-1} was fitted for the protein secondary structures using PeakFit software. The relative percentages of different protein secondary structures were calculated based on the integrated peak areas.

2.14. Preparation and formulation of Frankfurt sausages

Traditional sausages (control group) were prepared using lean meat, pork back fat, ice, salt, and sodium tripolyphosphate. In the low - fat Frankfurt sausages, EPS - EWP composite gel was used to replace an equivalent mass of pork back fat. Following the method by Rezaee and Aider (2023), lean meat and pork back fat were separately ground using a grinder, and the EPS - EWP composite gel was fragmented into gel particles using a homogenizer for 2 min. The pork back fat and EPS - EWP composite gel particles were mixed, 5 g of ice water were added, and the mixture was homogenized at 3000 r/min for 2 min to form a gel emulsion. The lean meat, gel emulsion, remaining ice water, and other ingredients were then emulsified using a silent cutter mixer. Afterward, the meat paste was stuffed into pork casings using a sausage stuffer. The sausages were cooked in 90 °C water for 30 min. Each batch of sausage need to be measured for cooking loss. The remaining sausages were then vacuum-packed and stored in a refrigerator at 4 °C until analysis. Three independent batches of sausages were prepared on different days, and each batch included three sausages for each measurement.

2.15. Cooking loss of sausages

According to the method described by Li et al. (2022), the meat paste was filled into casings to obtain the initial weight of the raw sausages, W_1. The sausages are then heated at 90 °C for 30 min, followed by a 1 h cooling period. After gently wiping the sausages, they were weighed again, noted as W_2. The weight loss due to cooking was calculated using the following formula:

$$\text{Cooking Loss Rate } (\%) = \frac{W_1 - W_2}{W_1} \times 100\%$$

2.16. pH changes in sausages

The measurement of pH changes were conducted based on the method described by Hayes et al. (2010), with slight modifications. After cooking, the sausage samples were minced and homogenized with distilled water at a ratio of 1: 10. The pH of the samples was then determined using a pH meter equipped with a pH electrode. Calibration was performed by immersing the electrode in standard buffer solutions with pH values of 4, 7, and 10 until the display stabilized, and the readings were adjusted accordingly to these values. The pH values of six groups of samples were measured on day 0, 4, and 8, with each measurement repeated three times.

2.17. fat oxidation analysis

The TBARS value was determined using the method described by

Deng et al. (2021). The sample was thoroughly mixed, with 2 g of the mixture combined with 3 mL of 1 % TBA solution and 17 mL of 2.5 % TCA - HCl solution. A few drops of butylated hydroxytoluene were added to the mixture before heating in boiling water for 30 min, followed by cooling to room temperature. The mixture was then blended with an equal volume of trichloromethane for 1 min and centrifuged at 3000 rpm for 10 min. The absorbance of the supernatant was recorded at a wavelength of 532 nm. The TBARS value was calculated based on the dilution factor and the molar extinction coefficient "9.48, 152,000 $M^{-1}cm^{-1}$", expressed in mg MDA/kg.

2.18. electronic nose analysis of sausages

The PEN3 electronic nose was utilized for the measurements, with the detector calibrated and prepared in advance. Precisely weigh 10 g of the chopped sample and place it in a 20 mL brown headspace vial. Subsequently, incubate the sample in a water bath at 60 °C for 20 min, followed by a 10 - min equilibrium period at room temperature (25 °C). Measurements were conducted using a disposable syringe needle. The electronic nose analysis parameters were as follows: sampling interval of 5 s, cleaning time of 90 s, zeroing time of 10 s, measurement time of 180 s, and a flow rate of 150 mL/min. The data were processed and principal component analysis plots were generated, with each sample measured three times.

2.19. sensory evaluation of sausages

The sensory evaluation panel consisted of 20 laboratory members with sensory evaluation experience. They rated the sausages based on color, density, texture, flavor, and overall acceptability, with each category having a maximum score of 7 points, and results were rounded to one decimal place. According to Fontes - Candia et al. (2023), the relationship between the back fat content in sausages and their texture, flavor, and appearance scores was analyzed. The evaluators tested six groups of sausage samples once a day for 3 d. Before tasting different groups of sausages, they rinsed their mouths with mineral water to avoid influencing the results.

2.20. data processing

The results were presented as the mean values from three replicates with standard errors. Experimental data were statistically analyzed using SPSS 26 (SPSS Inc., USA). Data on chemical components and physicochemical properties were analyzed by one-way analysis of variance (ANOVA). Duncan's multiple range test were employed for mean comparisons, and differences were considered significant at $P < 0.05$.

3. Results and discussion

3.1. Characteristics of EPS - EWP composite gel

3.1.1. Influence of EPS addition on the texture properties of composite gel

The hardness and elasticity parameters of the composite gel obtained through TPA testing are shown in Fig. 2A. The incorporation of EPS had a significant impact on the hardness and elasticity of the EPS - EWP composite gel ($P < 0.05$). Specifically, the hardness and elasticity of the thermally induced composite gel exhibited an initial increase followed by a subsequent decrease with increasing amounts of added EPS. The maximum values of hardness and elasticity were achieved when 0.6 % of EPS was added, measuring at 223.46 g and 0.83 g respectively. The three - dimensional network structure formed by EWP plays a crucial role in maintaining the performance of gels, and the incorporation of polysaccharides serves as a significant approach to enhance the strength of EWP gels (Nicoleti & Telis, 2009). According to Ma et al. (2022), polysaccharides can enhance the interactions among protein molecules, leading to the formation of a more robust network structure. As a result, this increases the hardness and elasticity of the composite gel. However, an excessive number of EPS can result in electrostatic repulsion with proteins, thereby impeding the formation of the gel network structure. The excessive binding of EWP and EPS involves a higher proportion of hydrophobic amino acids in covalent reactions, leading to reduced hydrophobicity and consequently compromising the hardness of the gel (Sun, Mu, et al., 2020).

3.1.2. The impact of EPS addition on the color difference of composite gels

The data presented in Fig. 2B visually demonstrates that the composite gel achieves its maximum L* brightness in the absence of added EPS. Upon the addition of EPS, there was a decrease in L* value, and the a* value initially increased followed by a subsequent decrease, while the b* value gradually increased. When using the EWP gel without adding EPS as a control, the total color difference ΔE of the gels with added EPS was approximately 6 units, with no statistically significant differences observed among the components ($P > 0.05$). This may be attributed to potential Maillard reactions occurring between EPS and EWP, resulting in some degree of browning (Biswas et al., 2022).

3.1.3. Effect of EPS addition on the water - holding capacity (WHC) of composite gels

The WHC of EWP gels and composite gels was assessed by incorporating different quantities of EPS additives and subjecting them to centrifugation. The composite gels of EPS - EWP demonstrated significantly enhanced water - holding capacity in comparison to the single EWP gels, as illustrated in Fig. 2C. Notably, the composite gel containing 0.6 % EPS displayed the highest water-holding capacity (94.67 %), representing a remarkable increase of 18.83 % compared to the EWP gel ($P < 0.05$). The observed improvement can likely be attributed to the robust activity of hydroxyl groups and the hydrophilicity of EPS, as well as a reinforced gel network that provides an enhanced environment for increased water retention (Khemakhem et al., 2019). However, when the EPS content reached 0.8 %, the gel structure was damaged due to molecular forces, leading to easier loss of water.

3.1.4. Impact of EPS addition on the interaction forces in composite gels

Fig. 2D illustrates that ionic bonds, hydrogen bonds, hydrophobic interactions, and disulfide bonds are the primary chemical forces associated with the network structure of EWP gels. These four types of forces initially increased and then slightly decreased upon the addition of EPS, indicating that an optimal quantity of EPS can enhance intermolecular interactions among protein molecules. The EWP molecules exhibited a multitude of exposed hydrophobic groups on their molecular surface following heat - induced denaturation, resulting in intermolecular cross - linking between protein molecules. Furthermore, covalent cross - linking occurred between EPS and EWP, thereby augmenting the structural stability of the protein molecules (Xia et al., 2022).

3.1.5. Influence of EPS addition on the microstructure of composite gels (SEM)

Fig. 2E illustrates the microstructures of EWP and various EPS - EWP composites. Compared to the control EWP gel, the composite gel exhibited smaller pore sizes and a denser structure, resulting in increased water storage capacity and enhanced capillary action for water adsorption. Particularly, the composite gel with 0.6 % EPS added showed a smoother and more uniformly dense structure. This suggested that EPS may crosslink with EWP, resulting in a denser gel network (Xia et al., 2022). The addition of more EPS resulted in an increase in the pore size of the composite gel network, which became irregular. This could be attributed to the electrostatic repulsion between EPS and proteins, as well as a decrease in intermolecular forces. The crosslinking and tight structure of protein molecules can enhance the gel's resistance to external stimuli and its WHC (Xiao et al., 2019). However, excessive interactions can lead to the opposite effect.

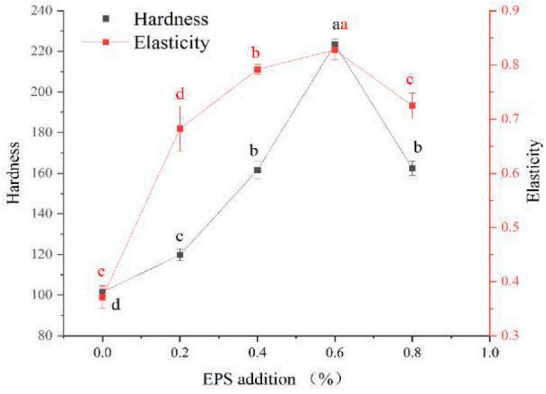

A

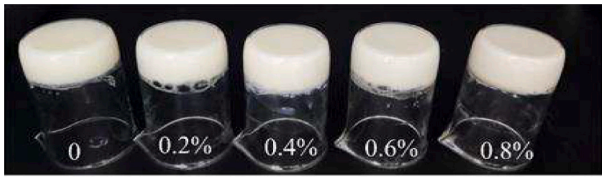

B

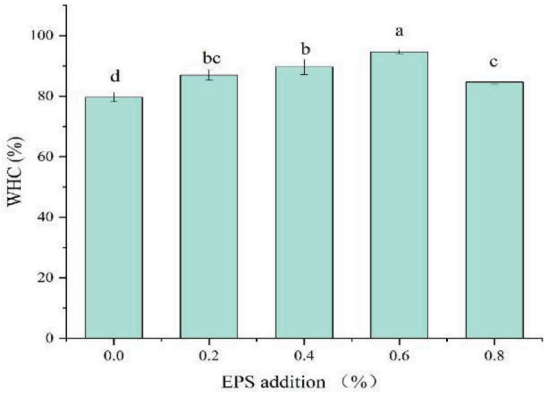

C

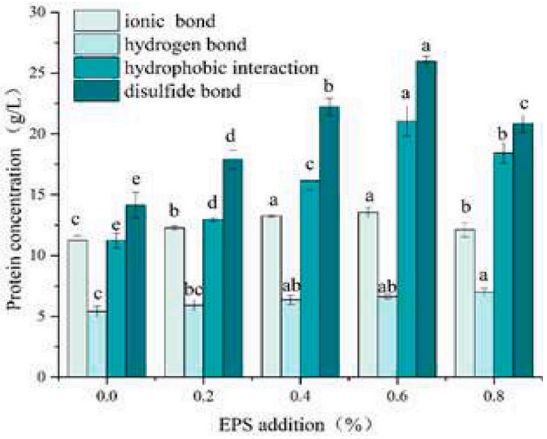

D

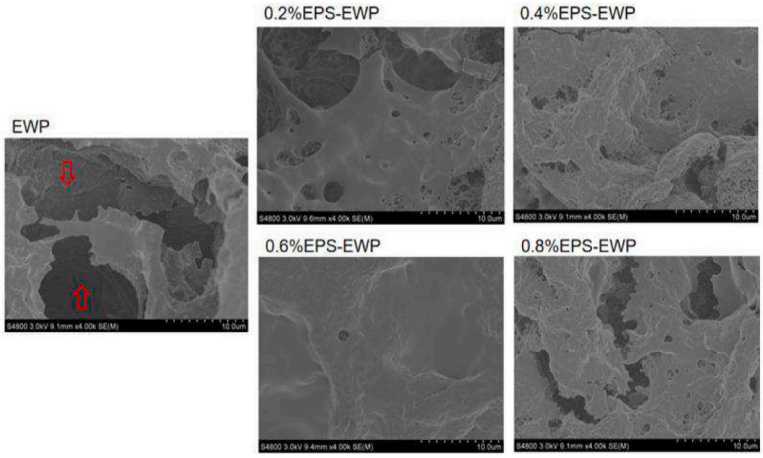

E

Fig. 2. Effect of different EPS addition on properties of composite gel. **A:** Hardness (black line) and elasticity (red line) of gels with different EPS addition: 0 % (0 % EPS - 8 % EWP gel), 0.2 % (0.2 % EPS - 8 % EWP composite gel), 0.4 % (0.4 % EPS - 8 % EWP composite gel), 0.6 % (0.6 % EPS - 8 % EWP composite gel) and 8 % (0.8 % EPS - 8 % EWP composite gel). Different lowercase letters indicate significant differences between groups ($P < 0.05$). **B:** Visual view of gel color difference of different EPS addition: 0 % (0 % EPS - 8 % EWP gel), 0.2 % (0.2 % EPS - 8 % EWP composite gel), 0.4 % (0.4 % EPS - 8 % EWP composite gel), 0.6 % (0.6 % EPS - 8 % EWP composite gel) and 8 % (0.8 % EPS - 8 % EWP composite gel). **C:** Water holding capacity of gels with different EPS addition: 0 % (0 % EPS - 8 % EWP gel), 0.2 % (0.2 % EPS - 8 % EWP composite gel), 0.4 % (0.4 % EPS - 8 % EWP composite gel), 0.6 % (0.6 % EPS - 8 % EWP composite gel) and 8 % (0.8 % EPS - 8 % EWP composite gel). Different lowercase letters indicate significant differences between groups ($P < 0.05$). **D:** Effect of different amounts of EPS added on the force of composite gel molecules: 0 % (0 % EPS - 8 % EWP gel), 0.2 % (0.2 % EPS - 8 % EWP composite gel), 0.4 % (0.4 % EPS - 8 % EWP composite gel), 0.6 % (0.6 % EPS - 8 % EWP composite gel) and 8 % (0.8 % EPS - 8 % EWP composite gel). Different lowercase letters of the same color indicate significant differences between groups ($P < 0.05$). **E:** Microstructure diagram of the composite gel with different EPS addition (4000 ×): 0 % (0 % EPS - 8 % EWP gel), 0.2 % (0.2 % EPS - 8 % EWP composite gel), 0.4 % (0.4 % EPS - 8 % EWP composite gel), 0.6 % (0.6 % EPS - 8 % EWP composite gel) and 8 % (0.8 % EPS - 8 % EWP composite gel). (For interpretation of the references to color in this figure legend, the reader is referred to the web version of this article.)

3.1.6. Construction of protein models based on molecular docking technology

As ovalbumin is the primary protein in EWP, comprising 54 % of the total protein content, it is utilized as the receptor protein (Xia et al., 2022). MD technology was employed to simulate the non - covalent binding of ovalbumin with EPS. The intermolecular forces between ovalbumin and EPS molecules, as predicted by PLIP programs in Fig. 3A, are depicted, emphasizing the presence of robust hydrophobic interactions and hydrogen bonds on the target protein ovalbumin. This indicated a high level of stability in the binding process (Zang et al., 2023a). In the proposed model (Fig. 3A), EWP - EPS predominantly interacted with specific amino acid residues within ovalbumin, particularly lysine (Lys) and aspartic acid (Asp), demonstrating a highly favorable docking energy of −8.30 kJ/moL, indicating a stable interaction.

The observed reduction in disordered structures in FTIR analysis, along with the enhanced WHC and measured intermolecular forces, provide further evidence for significant hydrophobic interactions and hydrogen bonding between EWP and EPS, which aligns with the findings from MD.

The dynamic stability of the system was verified by conducting a 100 ns MD simulation of the complex to investigate the interaction between the receptor protein, OVA, and EPS during motion and assess the stability of binding sites. The Root Mean Square Deviation (RMSD) is a crucial metric for assessing the attainment of equilibrium in a complex system. The RMSD of the complex system was depicted in Fig. 3B. Following approximately 50 ns of MD simulation, the system - initiated stabilization. Furthermore, as evidenced by Fig. 3B, the RMSD value of the isolated OVA system exhibited notable fluctuations at around 70 ns, indicating an abrupt structural transition. This phenomenon was absent in the complex, underscoring EPS's effective role in stabilizing the structure of OVA and yielding a more robust protein (Wu et al., 2019).

The radius of gyration (Rg) can be used to measure the compactness of a protein (Lee, 2024). The difference in Rg values can visually reflect the density and stability of the protein structure, with a smaller difference indicating a more compact and stable structure. The data from Fig. 3C clearly demonstrated an initial increase in Rg values followed by a gradual decrease and stabilization over time for each system. Specifically, the Rg of the 01 - system stabilized within the range of 3.58–3.62 nm. This observation suggested that the protein exhibited excellent fluidity and extensibility during simulation.

The hydrophobicity of amino acid residues is a crucial factor affecting protein folding (Lou et al., 2024), and the solvent - accessible surface area (SASA) is an important parameter to describe protein hydrophobicity. The hydrophobic amino acids in protein structures are typically situated within the protein, away from solvents. As depicted in Fig. 3D, the buried surface area of the OVA - EPS system remained consistently around 3.6 nm^2, indicating a significant role of hydrophobic residues in protein folding through the formation of a hydrophobic core that contributes to maintaining protein stability (Pan et al., 2024).

Hydrogen bonds are known to play a key role in stabilizing protein-ligand interactions (Zhu et al., 2019). From Fig. 3E, the number of hydrogen bonds in the OVA - EPS system was found remained relatively stable throughout the 100 ns simulation. These fluctuations may be influenced by interactions among different types of hydrogen bonds, which can vary in distance, angle, and bond energy. The relatively stable number of hydrogen bonds in the OVA - EPS system might reflect more consistent interactions.

As shown in Fig. 3F, MM - PBSA analysis is an effective approach for studying the key interactions between ligands and protein targets (Rout et al., 2021). By conducting an analysis of the individual amino acid residues' contribution to the binding free energy, valuable insights can be gained regarding the mechanism and identification of crucial residues involved in ligand binding. In this study, we performed energy decomposition analysis on key amino acid residues at the active site involved in ligand binding. The results indicated that the OVA - EPS complex exhibited a positive total binding free energy (Etotle) of 8.27 kJ, suggesting that external conditions were necessary for successful ligand binding. The binding free energy was decomposed into four components: van der Waals energy (EVDW), electrostatic energy (Eele), polar solvation energy (EPA), and SASA energy (ESA). This enabled us to obtain a comprehensive understanding of the critical interaction energies during the binding process.

As depicted in Fig. 3G, both EVDW and ESA energies exhibited negative values, indicating their favorable contributions to the binding process; whereas solvation energy demonstrated a positive value, suggesting its opposing effect on binding. Furthermore, Fig. 3G illustrated the energetic role played by amino acids in facilitating the interaction between OVA and EPS.

The Gibbs free energy landscape is utilized to illustrate the conformation with the lowest energy throughout the molecular dynamics simulation of the complex structure (Zaferani et al., 2024). If the protein-ligand interaction is weak or unstable, the free energy landscape will display multiple rough and low - energy clusters on its surface. Conversely, strong and stable interactions can result in an almost singular and smooth energy cluster within the potential energy distribution. As shown in Fig. 3H, the blue spots reflected the minimum energy values, indicating the most stable structures. The OVA - EPS complex had a concentrated low-energy region, suggesting a stable binding area between OVA and EPS.

3.1.7. Impact of EPS addition on the rheological properties of composite gels

Fig. 4A depicts the impact of different levels of EPS addition on the apparent viscosity of EPS - EWP composite gels. The increase in EPS content demonstrated a positive correlation with the rise in apparent viscosity, reaching its peak at an EPS concentration of 0.6 %. Subsequent increments in EPS content resulted in a slight decrease in apparent viscosity. Furthermore, the apparent viscosity of different EPS-EWP composite gels significantly decreased as the shear rate increased, indicating pseudoplastic behavior and shear thinning.

Dynamic frequency scans of the gels are shown in Figs. 4B and C. Both the EWP and EPS - EWP composite gels exhibited similar trends in their loss modulus (G") and storage modulus (G') curves, with G' consistently exceeding G", indicating the formation of elastic gels (Anvari & Tabarsa et al., 2016). Within the entire measured frequency range, G' played a predominant role over G", demonstrating solid-like behavior (Du et al., 2019). The addition of EPS led to an increase in both G' and G", which can be attributed to the unfolding of protein molecules during heating. This unfolding process, facilitated by the presence of EPS, resulted in the formation of intricate structures and promoted inter-protein cross-linking, ultimately enhancing the modulus values (Anvari & Chung, 2016). As the EPS content increased, more intermolecular regions participated in non - covalent cross - linking processes, resulting in increased viscosity. The formation of the largest connective region at an EPS concentration of 0.6 % indicates the presence of a distinct intermolecular network with robust gel properties, which is consistent with our findings regarding hardness. Tan δ values greater than 1 indicate predominantly viscous behavior, whereas values less than 1 suggest elastic characteristics. The tan δ values, ranging from 0.1 to 1.0 as depicted in Fig. 4D, indicate that the EPS - EWP composite gels predominantly exhibit elastic characteristics. Notably, the addition of 0.6 % EPS results in the most pronounced elasticity.

3.1.8. Impact of EPS addition on the moisture distribution in composite gels (LF - NMR)

The effect of different EPS addition levels on the moisture distribution of EPS -EWP composite gels is shown in Fig. 5A. This figure reflects the moisture distribution and migration state within the gels and explains the intrinsic reasons for changes in gel WHC (Han et al., 2014). The results indicated that the immobile water represented by T_{21} was responsible for the primary moisture distribution within the gel. The

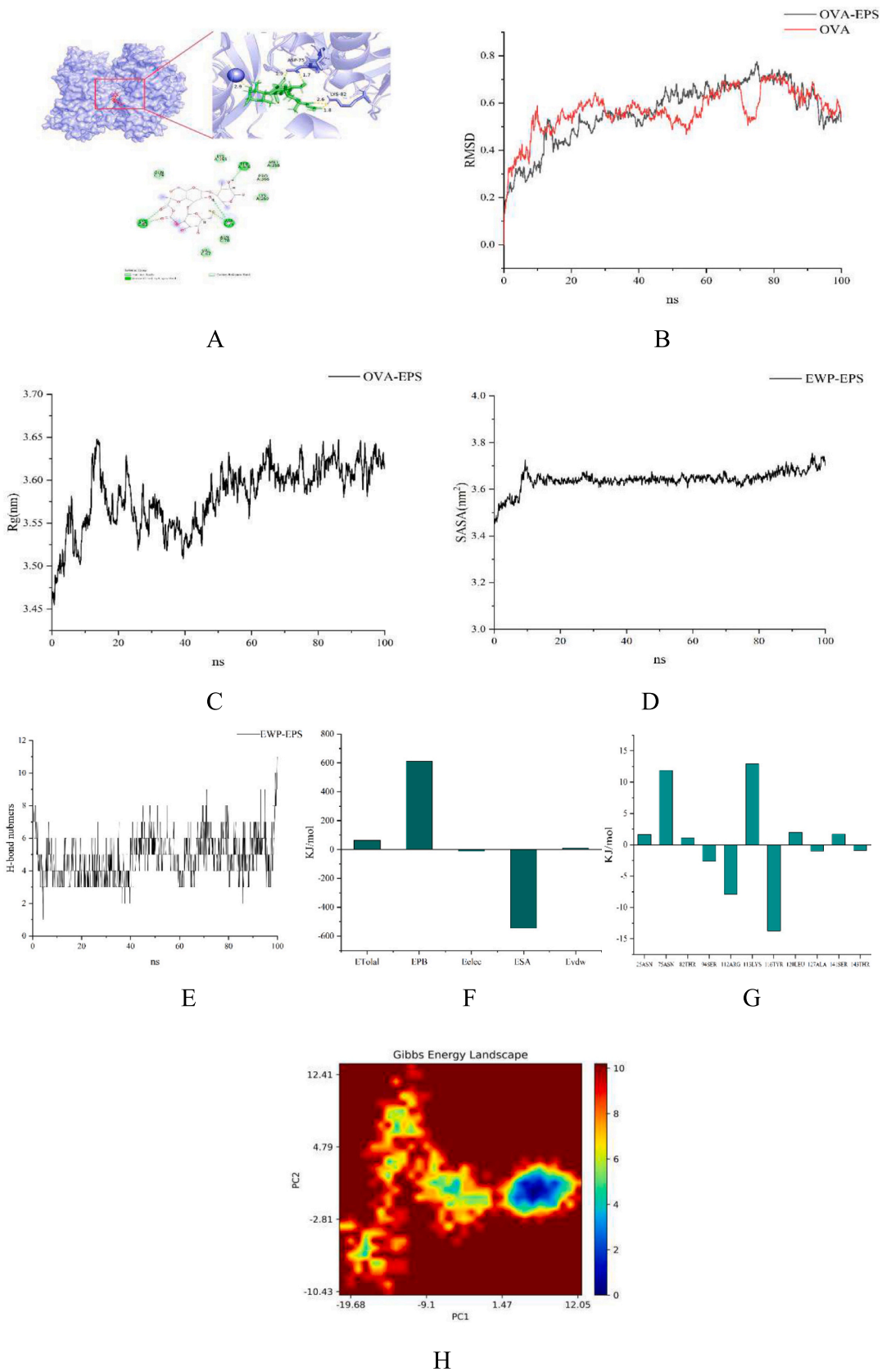

Fig. 3. Molecular docking between ovalbumin and EPS. **A:** The 3 - dimensional molecular docking images of ovalbumin and EPS. Where the blue bars represent amino acid residues in ovalbumin that interact with the EPS molecule, and the green - red bars are the EPS molecule. Note: where the blue bars represent amino acid residues in ovalbumin that interact with the EPS molecule, and the green - red bars are the EPS molecule. **B:** RMSD. **C.** Rg. **D.** SASA. **E.** H - bonds numbles. **F**: Binding free energy of single amino acid residue pair. **G**: Energy produced by amino acids in combination. **H:** Gibbs engergy landscape. (For interpretation of the references to color in this figure legend, the reader is referred to the web version of this article.)

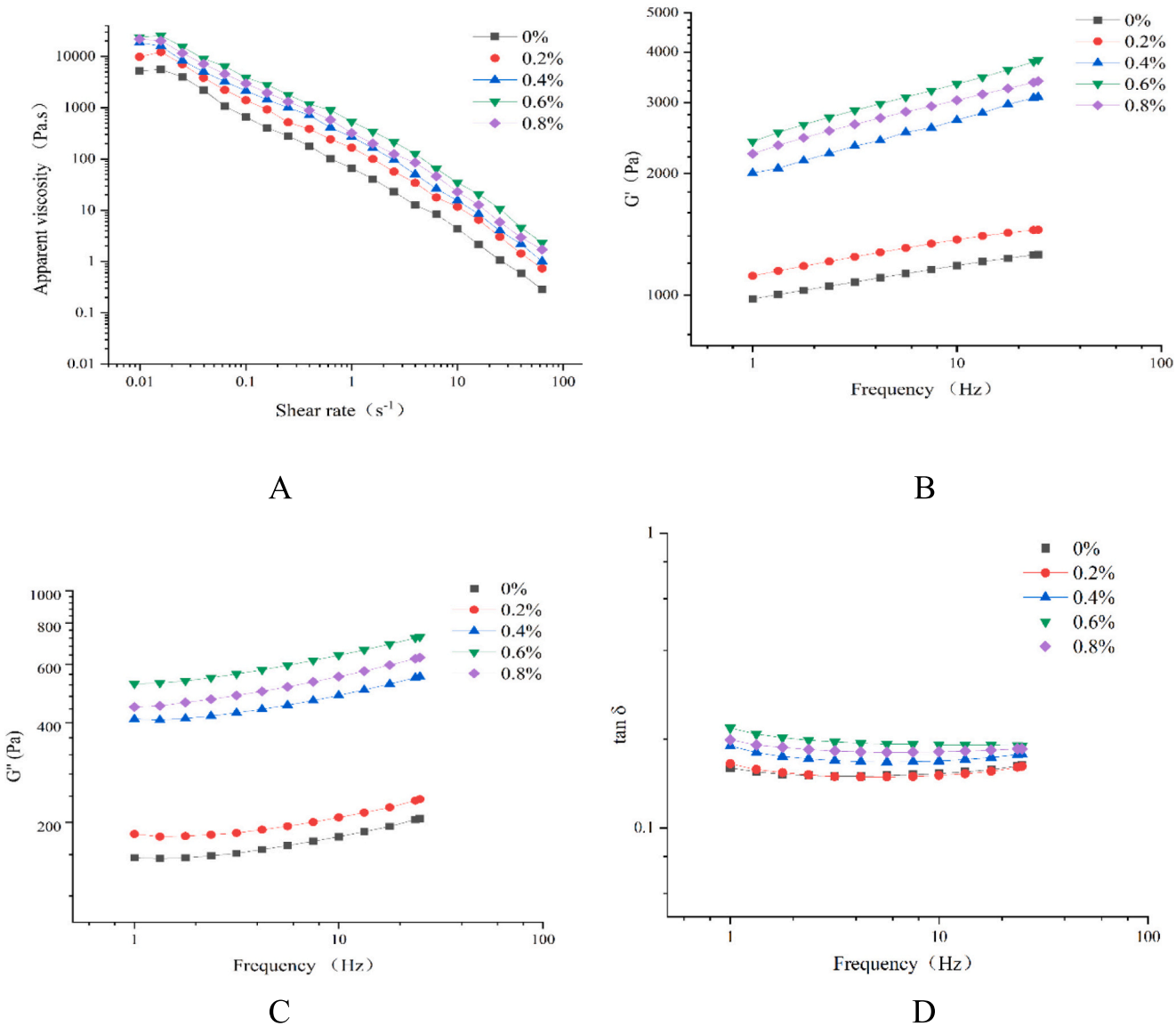

Fig. 4. Effect of EPS addition on rheological properties of composite gel. **A:** Effect of different EPS additions on the apparent viscosity of composite gel. **B:** Energy storage modulus of composite gel (G′) with different EPS addition amounts. **C:** Loss modulus (G″) of composite gel with different EPS addition. **D:** Loss angle of composite gel with different EPS addition. 0 % (0 % EPS - 8 % EWP gel), 0.2 % (0.2 % EPS - 8 % EWP composite gel), 0.4 % (0.4 % EPS - 8 % EWP composite gel), 0.6 % (0.6 % EPS - 8 % EWP composite gel) and 8 % (0.8 % EPS - 8 % EWP composite gel).

transverse relaxation time, T_2, as shown in Fig. 5B, exhibited a trend of initially decreasing and then increasing, with the shortest T_2 observed at an EPS addition of 0.6 %, indicating a stronger binding force to water molecules in the composite gel at this concentration. The shift towards shorter relaxation times is attributed to an increase in the gel's attraction to water molecules (Xia et al., 2018). Possible reasons may include the potential role of polysaccharides in filling gaps within the gel matrix and enhancing the egg white proteins' ability to retain moisture, thereby accounting for the observed improvement in water holding capacity (WHC) of the samples. The network structure restricts the flow of water molecules, promoting spin exchange with surrounding water molecules and leading to a reduction in spin relaxation time (T_2) (Zhang et al., 2016). Additionally, capillary action plays a crucial role in minute pores, securely trapping water, resulting in a steady state of liquid retention. Conversely, water molecules in larger cavities are unstable and easily lost with external force intervention (Farjami et al., 2015). The highest proportion of bound water and the lowest of free water at 0.6 % EPS - EWP explained the pattern observed in WHC. By enhancing intermolecular interactions and increasing the hydration shell, adding EPS to EWP increases the peak area of bound water and decreases that of free water (Xia et al., 2018).

3.1.9. Effect of EPS addition on the secondary structure of composite gels (FTIR)

The FTIR spectra of the composite gels are presented in Fig. 5C, where the wavelengths ranging from 3500 to 3000 cm^{-1} correspond to the FT - IR water region (grey shaded). This region primarily encompasses vibrations of hydrated and non-hydrated protein - OH and - NH_2 groups, which serve as indicators for protein-water interactions. Additionally, the wavelength at 2800 cm^{-1} corresponds to stretching vibrations of - CH bonds. The amide I region (1700–1600 cm^{-1}, green shaded) relates to the stretching vibrations of the C = O bonds (1800–1600 cm^{-1}) (Antony et al., 2022; Nagarajan et al., 2012). After the addition of 0.6 % EPS, the absorption peak at 3277.73 cm^{-1} shifted to 3200.87 cm^{-1}, moving towards lower wavenumbers. Indeed, lower peak wavenumbers suggest stronger protein-water interactions (Sinthusamran et al., 2017).

The amide I band (1700–1600 cm^{-1}) is a sensitive area within the

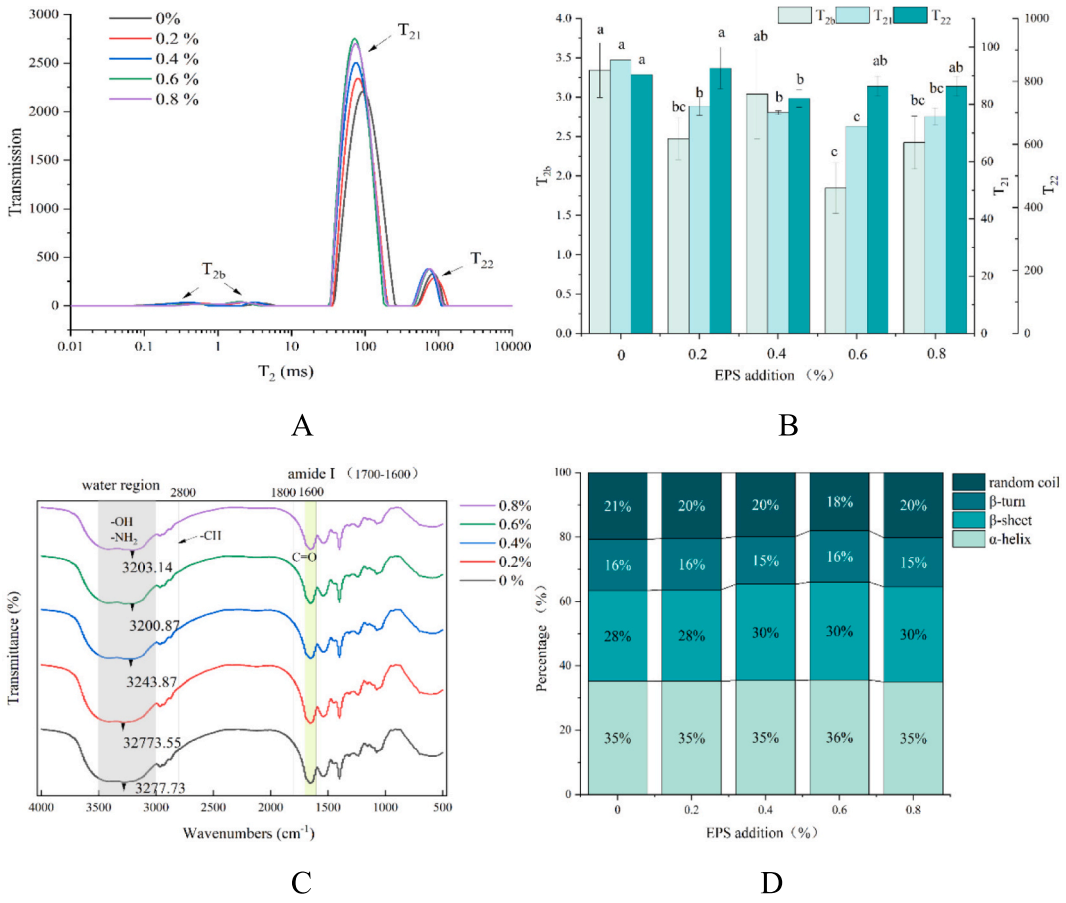

Fig. 5. Effect of EPS addition on water distribution and secondary structure of composite gel. **A:** Moisture distribution of composite gels with different EPS additions. **B:** Lateral relaxation time of composite gels with different EPS additions T_2. 0 % (0 % EPS - 8 % EWP gel), 0.2 % (0.2 % EPS - 8 % EWP composite gel), 0.4 % (0.4 % EPS - 8 % EWP composite gel), 0.6 % (0.6 % EPS - 8 % EWP composite gel) and 8 % (0.8 % EPS - 8 % EWP composite gel). Different lowercase letters of the same color indicate significant differences between groups ($P < 0.05$) **C:** Infrared spectra of composite gels with different EPS addition amounts. **D:** Protein secondary structure percentage of composite gels with different EPS addition amounts. 0 % (0 % EPS - 8 % EWP gel), 0.2 % (0.2 % EPS - 8 % EWP composite gel), 0.4 % (0.4 % EPS - 8 % EWP composite gel), 0.6 % (0.6 % EPS - 8 % EWP composite gel) and 8 % (0.8 % EPS - 8 % EWP composite gel). Different lowercase letters of the same color indicate significant differences between groups ($P < 0.05$).

secondary structure of proteins, mainly used to determine the C = O and C = H stretching vibrations within protein structures (Antony et al., 2022). Changes in α - helix (1665–1645 cm^{-1}), β - sheet (1637–1600 cm^{-1}), β - turns (1700–1665 cm^{-1}), and random coils (1645–1637 cm^{-1}) are commonly used to assess changes in the protein's secondary structure. The formation of protein gel structures during thermal gelation is associated with α - helix and β - sheet structures (Liu et al., 2011). The proportions of α - helix and β - sheet exhibited an initial increase followed by a slight decrease with the addition of EPS, ultimately reaching their highest proportion at 0.6 % EPS, as depicted in Fig. 5D. The random coil conformation was minimized at 0.6 % EPS, while the orderly α - helix and β - sheet conformations were increased, resulting in an enhanced structural order of the composite gel (Zhang et al., 2023). Additionally, due to the unique structure of β - sheets, a higher proportion of β - sheets resulted in an increased extent of protein unfolding during heat induction, leading to enhanced exposure of hydrophobic groups. This augmented hydrophobic interaction facilitated complete binding between protein molecules prior to aggregation, thereby forming a more organized and compact network structure that maximized gel hardness (Zhang et al., 2023). This conclusion was consistent with the textural findings.

3.2. Impact of EPS - EWP composite gel as a fat replacer on sausage quality

3.2.1. Effect of composite gel as a fat substitute on the rheological properties of minced meat

The viscosity as a function of shear rate is depicted in Fig. 6A. With increasing shear rates, the apparent viscosity of all minced meat samples exhibited a significant decrease ($P < 0.05$), indicating pseudoplastic behavior of minced meat in sausages. An increase in substitution ratio resulted in an elevation of the apparent viscosity; however, complete substitution (substitution ratio of 100 %) led to a reduction in viscosity. This may be due to the high - viscosity gel - like structure of the polysaccharide-protein composite gel particles, which exhibit excellent stability against physical, chemical, and microbiological changes (Badar et al., 2023).

The storage modulus (G') and loss modulus (G") of minced meat with composite gel substitution are depicted in Fig. 6B and Fig. 6C, respectively. Within the measured frequency range, both G' and G" exhibited a gradual increase with frequency for all minced meat samples. Notably, the value of G' consistently surpassed that of G", indicating pronounced gel - like properties (solid - like behavior) across all minced meat samples (Du et al., 2019). Moreover, the G' and G" values of minced meat with different substitution ratios of composite gel particles were found to be higher than those of the control group (substitution ratio of 0 %), with the highest storage modulus observed at a substitution ratio of

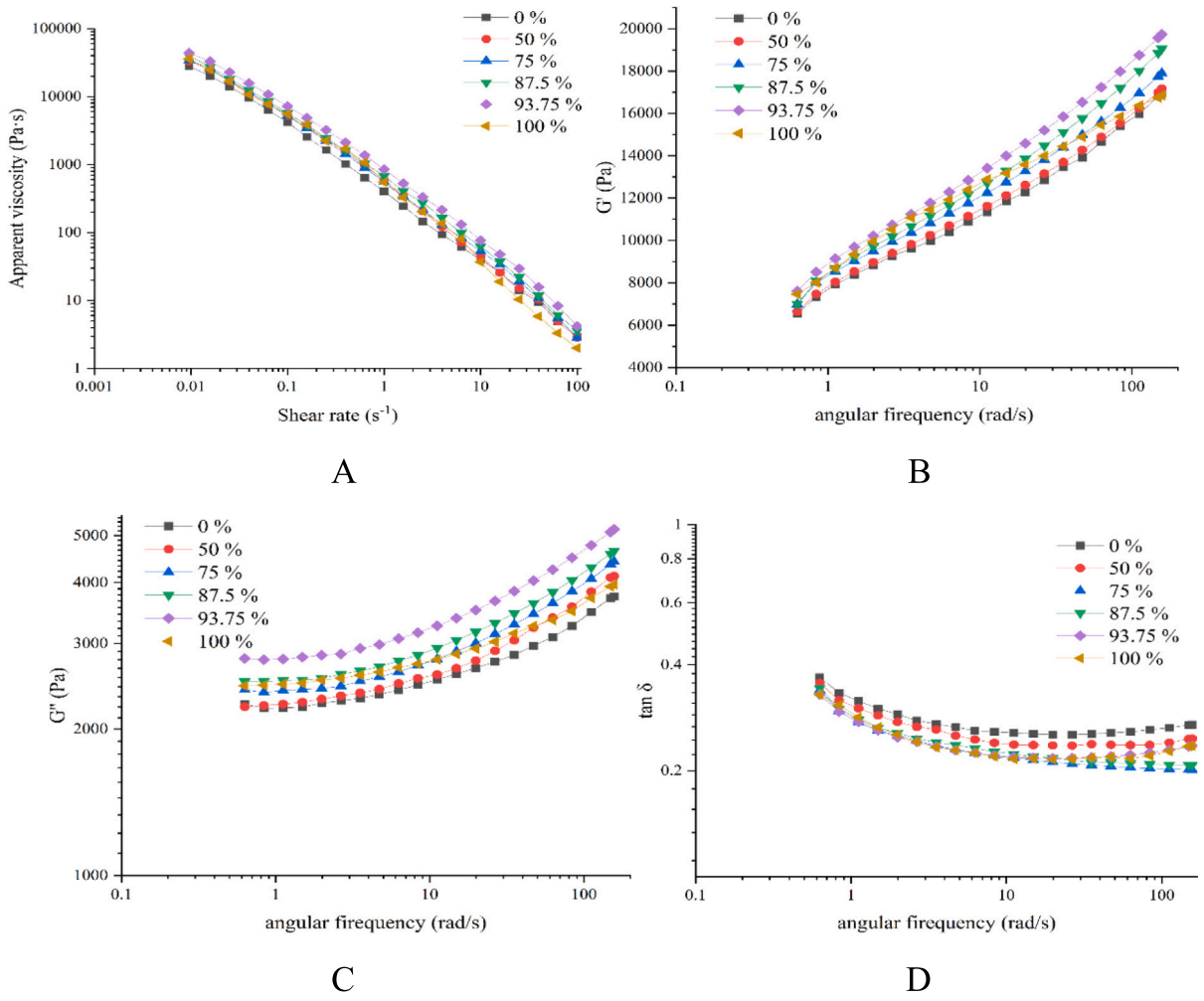

Fig. 6. Effect of different composite gel substitution ratios on rheological properties of meat. **A:** Effect of different composite gel substitution ratios on the apparent viscosity of minced meat. **B:** Effect of different composite gel substitution ratios on the energy storage modulus of minced meat. **C:** Effect of different composite gel substitution ratios on the modulus of loss of minced meat. **D:** Effect of different composite gel substitution ratios on tan δ of minced meat. Note: 0 % - 100 % in the graph indicates the composite gel substitution ratio, the same as below.

93.75 %. This observation suggested that minced meat containing composite gel particles retained favorable viscoelastic properties following shear deformation (Li et al., 2022). The effective filling of composite gel particles evidently enhances the muscle protein gel network, which can be attributed to the promotion of interactions between EWP and MP, as well as between lipids and water molecules. This leads to a uniform and orderly distribution of protein molecules and the formation of a dense and homogeneous gel network structure. Similar results have been reported previously (Gibis et al., 2015; C. Li et al., 2022). As depicted in Fig. 6D, a tan δ value greater than 1 primarily indicates the presence of viscous characteristics, while a tan δ value less than 1 is predominantly associated with elastic behavior. The range of tan δ values observed (0.1 to 1.0) suggests that all minced meat samples exhibited weak gel properties.

3.2.2. Effect of fat replacement by composite gels on cooking losses in sausages

The cooking loss in sausages is closely linked to the moisture distribution during the cooking process. As the substitution ratio of composite gel particles increased, a gradual decrease followed by a slight increase was observed in the cooking loss of sausages. Notably, the lowest cooking losses were recorded at substitution ratios of 87.5 % and 93.75 %, with no significant differences between these two groups (Fig. 7A) ($P < 0.05$). The inclusion of composite gels in sausages enhanced their WHC during heating, which was consistent with previous research on gel WHC. In this composite system, cooking loss was closely associated with the moisture content of raw meat as well as the levels of EWP and EPS (Rezaee et al., 2023). It is speculated that the reduction in cooking loss in sausages substituting pork back fat with EPS - EWP composite gel particles might be due to EPS's abundance of hydrophilic groups (– OH, – NH_2), which confer excellent water retention properties (Jiang et al., 2023). Moreover, EPS - EWP composite gel particles possess both hydrophilic and hydrophobic properties; the hydrophilic regions interact with water while the hydrophobic regions interact with oil. Additionally, their excellent mechanical strength improves the texture of sausages, facilitates moisture retention, and perfectly mimics the mouthfeel of fat. This makes them an ideal choice for replacing fat in meat products without affecting sensory attributes (Badar et al., 2023).

3.2.3. Impact of composite gel substitution for fat on fausage texture

Table 1 lists the textural characteristics of sausages prepared by substituting pork back fat with composite gel particles. Compared to the control group (0 % substitution), the substitution group showed significantly increased hardness and chewiness ($P < 0.05$), with minor changes in elasticity, cohesiveness, and resilience. At substitution levels of 87.5 % or 93.75 %, all textural parameters reached their highest values.

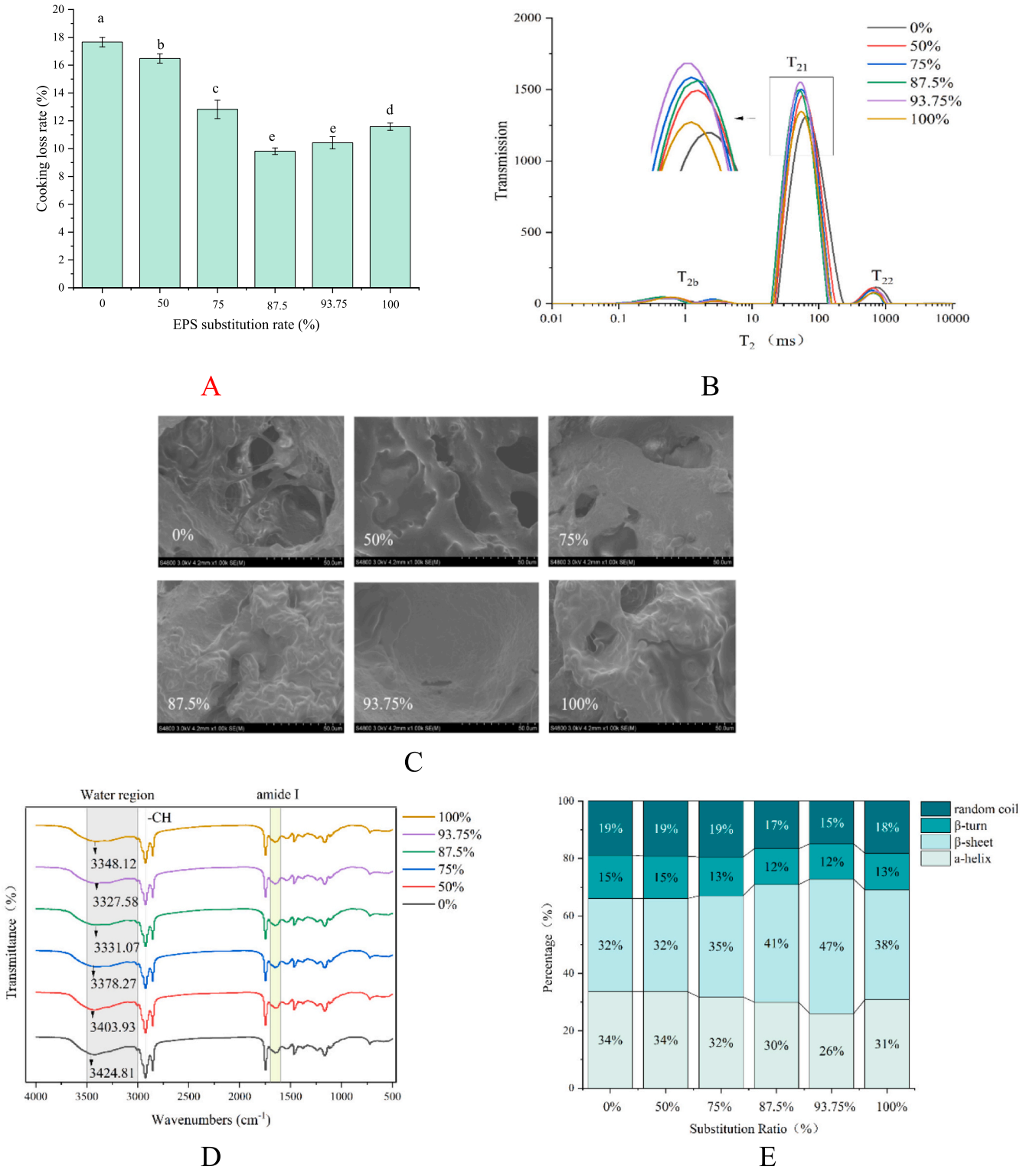

Fig. 7. Effect of compound gel replacing fat on sausage characteristics. **A:** Effect of different composite gel substitution ratios on sausage cooking loss. **B**: Effect of different composite gel substitution ratios on sausage water distribution. **C:** Microstructure diagram of sausage with different composite gel substitution ratios (1000 ×) **D:** FTIR profiles of sausages with different composite gel substitution ratios. **E:** proportion of secondary structure peak areas of sausages with different composite gel substitution ratios. Different lowercase letters of the same color indicate significant differences between groups ($P < 0.05$).

3.2.4. Impact of composite gel as a fat substitute on moisture distribution in sausages (LF - NMR)

LF - NMR is an effective technique for detecting different types of moisture content and mobility in meat products. As shown in Fig. 7B, the T_2 relaxation times exhibit three peaks, classified as T_{2b} (0–10 ms), T_{21} (10–100 ms), and T_{22} (100–1000 ms), representing bound water, immobilized water, and free water, respectively (Peng et al., 2020). Both T_{21} and T_{22} significantly shorten with an increase in the substitution ratio, reaching their shortest duration at a substitution ratio of 93.75 % ($P < 0.05$). Generally, T_2 reflects the mobility of water; shorter T_2

Table 1
Effect of different composite gels substitution ratios on sausage texture.

substitution ratio /%	hardness /g	elastin	cohesivenes	chewability	reversibility
0	5197.98 ± 629.71^{b}	0.92 ± 0.04^{b}	0.84 ± 0.04^{a}	4047.93 ± 690.9^{b}	0.48 ± 0.22^{ab}
50	5294.54 ± 318.80^{b}	0.96 ± 0.00^{a}	0.88 ± 0.03^{a}	4516.62 ± 443.0^{ab}	0.52 ± 0.27^{a}
75	5545.26 ± 463.30^{ab}	0.95 ± 0.20^{ab}	0.84 ± 0.02^{a}	4366.36 ± 302.7^{ab}	0.42 ± 0.07^{b}
87.5	6124.70 ± 163.71^{a}	0.95 ± 0.13^{ab}	0.86 ± 0.03^{a}	4781.37 ± 89.79^{a}	0.51 ± 0.12^{a}
93.75	6143.57 ± 93.96^{a}	0.94 ± 0.02^{ab}	0.88 ± 0.05^{a}	4865.70 ± 42.73^{a}	0.51 ± 0.13^{a}
100	5428.21 ± 141.95^{b}	0.95 ± 0.01^{ab}	0.85 ± 0.01^{a} v	4457.51 ± 184.39^{ab}	0.50 ± 0.20^{a}

Note: 0% - 100% in the table indicates the composite gel substitution ratio, the same as below. Values are expressed as mean ± standard of triplicate samples. Values with different lowercase superscripts within a column differ significantly ($P < 0.05$).

indicates lower mobility (Li et al., 2021). In this study, the changes in T_{21} and T_{22} might be associated with an increase in the water content of sausages due to the addition of composite gel particles (Kang et al., 2022). The results suggested that substituting pig back fat with composite gel particles significantly affected the moisture distribution in sausages, including a reduction in the proportion of free water and moisture mobility ($P < 0.05$).

3.2.5. Impact of composite gel substitution for fat on the microstructure of sausages (SEM)

The SEM images of sausages with different substitution ratios are shown in Fig. 7C. The control group (0 % substitution) did not contain composite gel particles, exhibiting a loose structure with larger pores and a rough surface. As the substitution ratio increased to 93.75 %, the microstructure of the sausages became increasingly compact and smooth. However, when the substitution ratio was further increased to 100 %, the structure became loose again. Composite gel particles, compared to natural EWP, had a denser structure, smaller particle size, higher surface net charge, and greater surface hydrophobicity (Badar et al., 2023). The structural composition of this system plays a crucial role in minimizing cooking loss and improving gel properties, aligning with previous findings on cooking loss and gel texture. Furthermore, the authors observed that the incorporation of composite gel particles could augment the network structure of sausages, thereby facilitating homogeneity within the meat systems. The improved structure contributes to the limitation of cooking loss and enhancement of gel properties, which is consistent with previous findings on cooking loss and gel texture.

3.2.6. Impact of composite gel substitution for fat on the secondary structure of sausages (FTIR)

Fig. 7E reflected changes in the secondary structure of sausage proteins. α - helix and β - sheet structures were predominantly the highest proportion, and their total percentage increased with the substitution ratio when not fully substituted. Notably, the cumulative proportion of α - helix and β - sheet structures at a substitution ratio of 93.75 % was significantly higher compared to the control group ($P < 0.05$). Specifically, as the substitution ratio increased from 0 % to 93.75 %, there was a decreasing trend observed in the α - helix structure and a corresponding increase in β - sheet formation, ranging from 32 % to 47 %. Additionally, there was a significant reduction in β - turns and irregular curls ($P < 0.05$), indicating a transition towards an enriched presence of β - sheet structures (Zhang et al., 2021). The observed results suggested that the incorporation of gel led to a transition in the protein secondary structure within sausages, resulting in a shift from disordered to ordered states. Consequently, this modification significantly enhanced the cohesiveness of sausage proteins. Some articles have found that an increase in β-sheet content is associated with water retention (Herrero, 2008; Zhao et al., 2017). Therefore, based on the findings presented in Fig. 7E, it can be inferred that sausages with a substitution ratio of 93.75 % exhibit superior water retention properties, which is consistent with the conclusions drawn regarding sausage cooking loss.

3.2.7. Impact of composite gel substitution for fat on pH changes in sausages

The pH values of various sausage samples stored at 4 °C over a period of 8 d are depicted in Fig. 8A. The pH value exerted an influence on the functional and sensory attributes of sausages, including gel properties, WHC, and flavor. The findings revealed that at the onset of refrigeration (0 d), there was a statistically significant difference in pH values between sausages devoid of EPS - EWP composite gel (0 % substitution) and those with 50 % to 100 % substitution ($P < 0.05$). After 8 days of refrigeration, the pH values of all samples exhibited an increasing trend, with higher substitution ratios demonstrating a positive correlation with elevated pH levels. The recorded pH values for all samples fell within the range of 6.42 to 6.49, which coincides with the optimal pH range conducive to achieving enhanced emulsifying capacity in salt - soluble proteins extracted from common meats (Santhi et al., 2015). After more than a week of refrigeration, the pH values of all samples continued to rise.

3.2.8. Impact of composite gels substitution for fat on lipid oxidation in sausages

The TBARS method is commonly used to assess the lipid oxidation stability of meat products. The data presented in Fig. 8B demonstrated a positive correlation between the duration of storage and the accumulation of malondialdehyde (MDA), a byproduct resulting from fatty acid oxidation. Notably, the control group (0 % substitution ratio) exhibited significantly elevated MDA levels, indicating pronounced oxidative damage and degradation. The control group exhibited the highest MDA values, indicating elevated levels of oxidation and degradation. As the substitution ratio increased to 93.75 %, a gradual decrease in MDA content was observed, suggesting a lighter degree of lipid oxidation and an increasingly significant inhibitory effect on fat oxidation (Rezaee et al., 2023). This reduction was likely due to the decreased content of back fat in pork, which reduced the unsaturated fatty acids in the sausages, thereby diminishing the degree of oxidation (Patinho et al., 2020). Moreover, EPS exhibits a strong ability to scavenge hydroxyl radicals, inhibiting lipid oxidation (Wu et al., 2023). Significant differences were observed between groups with varying replacement ratios at the same storage duration ($P < 0.05$). The most effective inhibitory effects on lipid oxidation were seen at replacement ratios of 87.5 % and 93.75 %, showing a 32.87 % improvement compared to the control group. At a 100 % replacement ratio, the texture of the sausage may become loose and rough, increasing the surface area in contact with air, thus enhancing lipid oxidation. Composite gels as fat replacers in sausages hold great promise, potentially improving oxidative stability during refrigerated storage.

3.2.9. Impact of composite gel as a fat substitute on sausage data from an electronic nose

As shown in Fig. 8C, the contribution rate of PC1 was 77.4 % and that of PC2 was 12.6 %, resulting in a total contribution rate of 90 % for the two principal components. This observation indicates that these two principal components encompass the primary characteristic information regarding volatile compounds in pork sausages. Sausages with substitution ratios of 50 %, 75 %, 87.5 %, and 93.75 % exhibited overlapping profiles with the control group (0 % substitution), suggesting similar

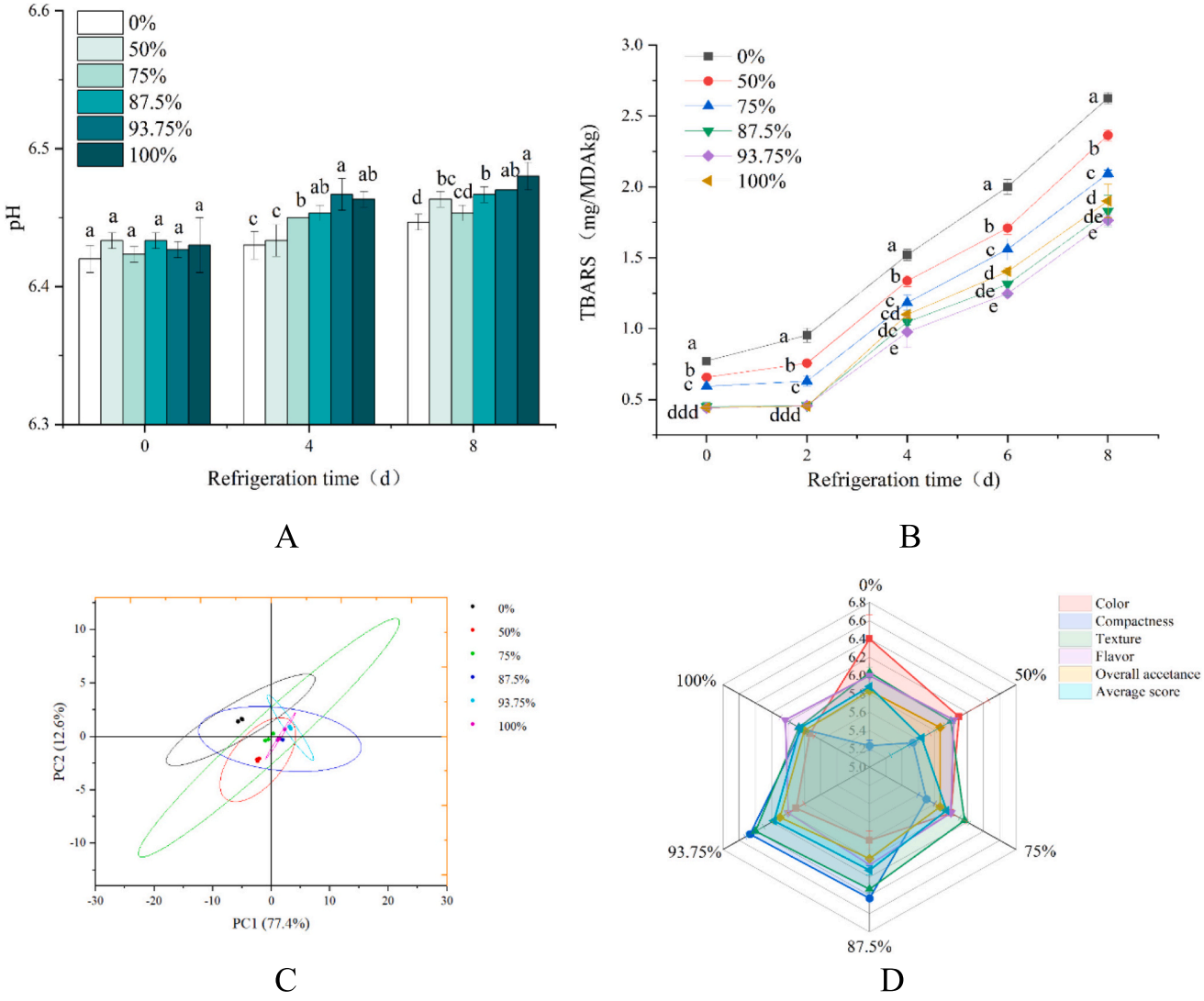

Fig. 8. **A:** Effect of different composite gel substitution ratios on sausage pH changes under short - term refrigeration. **B:** Effect of different composite gel substitution ratios under short - term RT on sausage TBARS values. **C:** Sausage PCA analysis of different composite gel substitution ratios. **D:** Sensory score radar chart of sausages with different composite gel substitution ratios. Different lowercase letters of the same color indicate significant differences between groups ($P < 0.05$).

overall odor characteristics. However, complete substitution at a ratio of 100 % displayed distinct separation from the control group while still overlapping with other groups. These findings imply that when the substitution ratio is below 93.75 %, there are no significant differences in odor between sausages ($P > 0.05$); however, complete fat substitution does lead to some changes in flavor profile. Therefore, composite gels can effectively replace most of the fat content, but complete substitution may have an impact on flavor.

3.2.10. Impact of composite gel fat substitution on sausage sensory characteristics

Based on the findings from Fig. 8D, it was evident that the color scores of the control group (substitution ratio 0 %) were significantly higher than those of the experimental groups. No significant differences in color scores were observed among the experimental groups ($P > 0.05$), which aligned with the results obtained for color difference indicators. This observation can be attributed to the impact of substituting fat with gel on the gloss and brightness of pork sausages. Notably, sausages with a substitution ratio of 93.75 % exhibited significantly higher compactness and texture scores compared to other treatment groups ($P < 0.05$). This improvement can be attributed to better dispersion of gel particles compared to fat, facilitating protein – water - fat interactions within the system and thereby enhancing sausage compactness and juiciness (Kim et al., 2020). The gel did not significantly enhance the flavor of the sausages but improved their overall acceptability, which was significantly higher than that of other treatment groups ($P < 0.05$). Notably, when the gel particles completely substituted pork back fat (substitution ratio 100 %), the sausage structure appeared rough and porous. In short, all sausages had average scores above 5.60, with the highest overall acceptability and average score observed at a substitution ratio of 93.75 %, indicating that the polysaccharide-protein composite gel could replace fat to achieve low-fat sausages with good acceptability.

4. Conclusion

Compared with single EWP gel, EPS - EWP composite gel containing 0.6 % EPS has significantly enhanced structural properties, water retention capacity and viscoelasticity. MD studies show that the main factors affecting the interaction between EWP and EPS are hydrogen bonding and hydrophobic power. The EPS - EWP composite gel can replace up to 93.75 % of the back fat in Frankfurters. Compared with the control sausage, the cooking loss of low - fat sausage was significantly reduced, and the hardness and chewiness were significantly increased.

After the composite gel replaced the mince, the viscoelasticity and storage modulus of the mince were enhanced, the structure was stable, the secondary structure of the protein changed from disorder to order, the protein - water interaction was enhanced, and the cohesion was enhanced. In addition, the bioactive EPS showed enhanced antioxidant capacity, thereby reducing lipid oxidation in the sausage. The low - fat sausage with a substitution rate of 93.75 % had good sensory properties compared to the control sausage, including unchanged color and a similar overall odor. Therefore, EPS - EWP composite gels have great potential in the development of low - fat sausages, both in line with the trend of healthy food choices, but also to meet consumer demand and social development.

Acknowledgements and Funding

This study was supported by the Anhui Provincial Department of Education collaborative innovation project [grant no. GXXT - 2023 - 051] and the 2021 Anhui Major Science and Technology Special Project [grant no. d06050001].

CRediT authorship contribution statement

Guoguo Jin: Writing – original draft, Methodology, Investigation. **Man Zhang:** Writing – original draft, Methodology, Investigation. **Xinran Wang:** Software. **Yifan Zhang:** Writing – original draft, Methodology. **Guohua Jiang:** Writing – original draft, Software. **Lin Mei:** Funding acquisition, Formal analysis, Conceptualization.

Declaration of competing interest

The authors declare that they have no known competing financial interests or personal relationships that could have appeared to influence the work reported in this paper.

Data availability

Data will be made available on request.

References

Abraham, M. J., Murtola, T., Schulz, R., Páll, S., Smith, J. C., Hess, B., & Lindahl, E. (2015). GROMACS: High performance molecular simulations through multi-level parallelism from laptops to supercomputers. *SoftwareX, 2015*(1–2), 19–25. https://doi.org/10.1016/j.softx.2015.06.00

Adachi, M., Takenaka, Y., Gidamis, A. B., Mikami, B., & Utsumi, S. (2001). Crystal structure of soybean proglycinin A1aB1b homotrimer. *Journal of Molecular Biology, 305*(2), 291–305. https://doi.org/10.1006/jmbi.2000.4310

Antony, J. V., Koya, R., Pournami, P. N., Nair, G. G., & Balakrishnan, J. P. (2022). Protein secondary structure assignment using residual networks. *Journal of Molecular Modeling, 28*(269). https://doi.org/10.1007/s00894-022-05271-z

Anvari, M., & Chung, D. (2016). Dynamic rheological and structural characterization of fish gelatin – Gum arabic coacervate gels cross-linked by tannic acid. *Food Hydrocolloids, 60*, 516–524. https://doi.org/10.1016/j.foodhyd.2016.04.028

Badar, I. H., Wang, Z., Liu, H., Chen, Q., Xia, X., Liu, Q., & Kong, B. (2023). Future prospects of high internal phase Pickering emulsions stabilized by natural modified biopolymers as a potential fat substitute in meat products. *Trends in Food Science & Technology, 40*(104176). https://doi.org/10.1016/j.tifs.2023.104176

Best, R. B., Zhu, X., Shim, J., Lopes, P. E. M., Mittal, J., Feig, M., & Mackerell, A. D. (2012). Optimization of the additive charmm all-atom protein force field targeting improved sampling of the backbone ϕ, ψ and side-chain χ_1 and χ_2 dihedral angles. *Journal of Chemical Theory and Computation, 8*(9). https://doi.org/10.1021/ct300400x

Bi, C.-H., Li, D., Wang, L.-J., & Adhikari, B. (2016). Effect of LBG on the gel properties of acid-induced SPI gels. *LWT - Food Science and Technology, 75*, 1–8. https://doi.org/10.1016/j.lwt.2016.08.028

Biswas, S., Melton, L. D., Nelson, A. R. J., Le Brun, A. P., Heinrich, F., McGillivray, D. J., & Xu, A. Y. (2022). The assembly mechanism and mesoscale architecture of protein–polysaccharide complexes formed at the solid–liquid interface. *Langmuir, 38*(41), 12551–12561. https://doi.org/10.1021/acs.langmuir.2c02003

Deng, S., Liu, Y., Huang, F., Liu, J., Han, D., Zhang, C., & Blecker, C. (2021). Evaluation volatile flavor compounds during storage time in bacon made by different pig breeds. *Food Chemistry, 357*, Article 129765. https://doi.org/10.1016/j.foodchem.2021.129765

Du, B., Fu, Y., Wang, X., Jiang, H., Lv, Q., Du, R., Yang, Y., & Rong, R. (2019). Isolation, purification, structural analysis and biological activities of water-soluble polysaccharide from Glehniae radix. *International Journal of Biological Macromolecules, 128*, 724–731. https://doi.org/10.1016/j.ijbiomac.2019.01.159

Elnahas, M. O., De León, K. B., Amin, M. A., Hussein, M. M. D., Ali, A. E., & Wall, J. D. (2017). Complete genome sequencing of *Streptomyces sp.* strain moe7, which produces an extracellular polysaccharide with antioxidant and antitumor activities. *Genome Announcements, 5*(22). https://doi.org/10.1128/genomea.00442-17

Farjami, T., Madadlou, A., & Labbafi, M. (2015). Characteristics of the bulk hydrogels made of the citric acid cross-linked whey protein microgels. *Food Hydrocolloids, 50*, 159–165. https://doi.org/10.1016/j.foodhyd.2015.04.011

Fu, X., Belwal, T., He, Y., Xu, Y., Li, L., & Luo, Z. (2020). Interaction and binding mechanism of cyanidin-3-O-glucoside to ovalbumin in varying pH conditions: A spectroscopic and molecular docking study. *Food Chemistry, 320*, Article 126616. https://doi.org/10.1016/j.foodchem.2020.126616

Gibis, M., Schuh, V., & Weiss, J. (2015). Effects of carboxymethyl cellulose (CMC) and microcrystalline cellulose (MCC) as fat replacers on the microstructure and sensory characteristics of fried beef patties. *Food Hydrocolloids, 45*, 236–246. https://doi.org/10.1016/j.foodhyd.2014.11.021

Guo, Y., Zhang, X., Hao, W., Xie, Y., Chen, L., Li, Z., Zhu, B., & Feng, X. (2018). Nano-bacterial cellulose/soy protein isolate complex gel as fat substitutes in ice cream model. *Carbohydrate Polymers, 198*, 620–630. https://doi.org/10.1016/j.carbpol.2018.06.078

Han, M., Wang, P., Xu, X., & Zhou, G. (2014). Low-field NMR study of heat-induced gelation of pork myofibrillar proteins and its relationship with microstructural characteristics. *Food Research International, 62*, 1175–1182. https://doi.org/10.1016/j.foodres.2014.05.062

Hayes, J. E., Stepanyan, V., Allen, P., O'Grady, M. N., & Kerry, J. P. (2010). Evaluation of the effects of selected plant-derived nutraceuticals on the quality and shelf-life stability of raw and cooked pork sausages. *LWT - Food Science and Technology, 44*(1), 164–172. https://doi.org/10.1016/j.lwt.2010.05.020

Herrero, A. M. (2008). Raman spectroscopy a promising technique for quality assessment of meat and fish: A review. *Food Chemistry, 107*(4), 1642–1651. https://doi.org/10.1016/j.foodchem.2007.10.014

Hoff, K. G., Silberg, J. J., & Vickery, L. E. (2000). Interaction of the iron-sulfur cluster assembly protein IscU with the Hsc66/Hsc20 molecular chaperone system of *Escherichia coli*. *Proceedings of the National Academy of Sciences of the United States of America, 97*(14), 7790–7795. https://doi.org/10.1073/pnas.130201997

Jiang, B., Chen, P., Guo, J., Han, B., Jin, H., Li, D., Liu, C., & Feng, Z. (2023). Structural characteristics and biological activity of lactic acid bacteria exopolysaccharides separated by ethanol/(NH4)2SO4 ATPS. *International Journal of Biological Macromolecules, 244*, Article 125451. https://doi.org/10.1016/j.ijbiomac.2023.125451

Jo, S., Kim, T., Iyer, V. G., & Im, W. (2008). CHARMM-GUI: A web-based graphical user interface for CHARMM. *Journal of Computational Chemistry, 29*(11), 1859–1865. https://doi.org/10.1002/jcc.20945

Josquin, N. M., Linssen, J. P. H., & Houben, J. H. (2011). Quality characteristics of Dutch-style fermented sausages manufactured with partial replacement of pork back-fat with pure, pre-emulsified or encapsulated fish oil. *Meat Science, 90*(1), 81–86. https://doi.org/10.1016/j.meatsci.2011.06.001

Kang, Z.-L., Xie, J.-J., Li, Y.-P., Song, W.-J., & Ma, H.-J. (2022). Effects of pre-emulsified safflower oil with magnetic field modified soy 11S globulin on the gel, rheological, and sensory properties of reduced-animal fat pork batter. *Meat Science, 198*, Article 109087. https://doi.org/10.1016/j.meatsci.2022.109087

Khemakhem, M., Attia, H., & Ayadi, M. A. (2019). The effect of pH, sucrose, salt and hydrocolloid gums on the gelling properties and water holding capacity of egg white gel. *Food Hydrocolloids, 87*, 11–19. https://doi.org/10.1016/j.foodhyd.2018.07.041

Klauda, J. B., Venable, R. M., Freites, J. A., O'Connor, J. W., Tobias, D. J., Mondragon-Ramirez, C., … Pastor, R. W. (2010). Update of the charmm all-atom additive force field for lipids: Validation on six lipid types. *The Journal of Physical Chemistry B, 114*(23), 7830–7843. https://doi.org/10.1021/jp101759q

Kumar, A. S., Mody, K., & Jha, B. (2007). Bacterial exopolysaccharides – A perception. *Journal of Basic Microbiology, 47*(2), 103–117. https://doi.org/10.1002/jobm.200610203

Lee, H. (2024). Hydrodynamics and aggregation of nanoparticles with protein corona: Effects of protein concentration and ionic strength. *Small*. https://doi.org/10.1002/smll.202403913

Li, Y. P., Kang, Z.-L., Sukmanov, V., & Ma, H.-J. (2021). Effects of soy protein isolate on gel properties and water holding capacity of low-salt pork myofibrillar protein under high pressure processing. *Meat Science, 176*, Article 108471. https://doi.org/10.1016/j.meatsci.2021.108471

Liu, R., Zhao, S.-M., Xie, B.-J., & Xiong, S.-B. (2011). Contribution of protein conformation and intermolecular bonds to fish and pork gelation properties. *Food Hydrocolloids, 25*(5), 898–906. https://doi.org/10.1016/j.foodhyd.2010.08.016

Loeffler, M., Hilbig, J., Velasco, L., & Weiss, J. (2020). Usage of in situ exopolysaccharide-forming lactic acid bacteria in food production: Meat products—A new field of application? *Comprehensive Reviews in Food Science and Food Safety, 19*(6), 2932–2954. https://doi.org/10.1111/1541-4337.12615

Lou, H., Wu, Y., Kuczera, K., & Schöneich, C. (2024). Coarse-grained molecular dynamics simulation of heterogeneous polysorbate 80 surfactants and their interactions with small molecules and proteins. *Molecular Pharmaceutics, 21*(10), 5041–5052. https://doi.org/10.1021/acs.molpharmaceut.4c00461

Lu, P., Mei, L., Wang, X., Wu, Y., Jin, G., & Zhang, M. (2024). Effects of exopolysaccharide by *Pediococcus acidilactici* S1 on the gelation properties and microstructure of porcine myofibrillar protein. *Food Hydrocolloids, 149*, Article 109627. https://doi.org/10.1021/10.1016/j.foodhyd.2023.109627

Ma, Y., Shan, A., Wang, R., Zhao, Y., & Chi, Y. (2021). Characterization of egg white powder gel structure and its relationship with gel properties influenced by pretreatment with dry heat. *Food Hydrocolloids*. https://doi.org/10.1016/j.foodhyd.2020.106149

Ma, Y., Zang, J., Qing, M., Xiao, Y., Zhang, H., Chi, Y., & Chi, Y. (2022). Glycosylation of egg white protein with maltodextrin in the dry state: Changes in structural and gel properties. *Food Chemistry, 401*, Article 134113. https://doi.org/10.1021/10.1016/j.foodchem.2022.134113

Mirarab Razi, S., Motamedzadegan, A., Shahidi, A., & Rashidinejad, A. (2018). The effect of basil seed gum (BSG) on the rheological and physicochemical properties of heat-induced egg albumin gels. *Food Hydrocolloids, 82*, 268–277. https://doi.org/10.1021/10.1016/j.foodhyd.2018.01.013

Nagarajan, M., Benjakul, S., Prodpran, T., Songtipya, P., & Kishimura, H. (2012). Characteristics and functional properties of gelatin from splendid squid (Loligo formosana) skin as affected by extraction temperatures. *Food Hydrocolloids, 29*(2), 389–397. https://doi.org/10.1021/10.1016/j.foodhyd.2012.04.001

Nicoleti, J. F., & Telis, V. R. N. (2009). Viscoelastic and thermal properties of collagen–xanthan gum and collagen–maltodextrin suspensions during heating and cooling. *Food Biophysics, 4*, 135–146. https://doi.org/10.1021/10.1007/s11483-009-9110-2

Pan, J., Xu, H., Dabbour, M., Mintah, B. K., Huang, L., Dai, C., … Ma, H. (2024). Changes in physicochemical, structural and functional properties, and lysinoalanine formation during the unfolding and refolding of pH-shifted black soldier fly larvae albumin. *International Journal of Biological Macromolecules, 272*(1). https://doi.org/10.1021/10.1016/j.ijbiomac.2024.132801

Patinho, I., Selani, M. M., Saldaña, E., Bortoluzzi, A. C. T., Rios-Mera, J. D., da Silva, C. M., … Contreras-Castillo, C. J. (2020). Agaricus bisporus mushroom as partial fat replacer improves the sensory quality maintaining the instrumental characteristics of beef burger. *Meat Science, 172*, Article 108307. https://doi.org/10.1021/10.1016/j.meatsci.2020.108307

Peng, Z., Zhu, M., Zhang, J., Zhao, S., He, H., Kang, Z., Ma, H., & Xu, B. (2020). Physicochemical and structural changes in myofibrillar proteins from porcine longissimus dorsi subjected to microwave combined with air convection thawing treatment. *Food Chemistry, 343*, Article 128412. https://doi.org/10.1021/10.1016/j.foodchem.2020.128412

Rezaee, M., & Aider, M. (2023). Study of the effect of canola proteins-xanthan based Pickering emulsion as animal fat replacer in a food matrix produced from mechanically separated meat. *Meat Science, 204*. https://doi.org/10.1021/10.1016/j.meatsci.2023.109283

Rombouts, I., Wouters, A. G. B., Lambrecht, M. A., Uten, L., Van Den Bosch, W., Vercruysse, S. A. R., & Delcour, J. A. (2020). Food protein network formation and gelation induced by conductive or microwave heating: A focus on hen egg white. *Innovative Food Science & Emerging Technologies, 66*. https://doi.org/10.1021/10.1016/j.ifset.2020.102484

Rout, J., Swain, B. C., Subadini, S., Mishra, P. P., Sahoo, H., & Tripathy, U. (2021). Conformational dynamics of myoglobin in the presence of vitamin B12: A spectroscopic and in silico investigation. *International Journal of Biological Macromolecules, 192*, 564–573. https://doi.org/10.1016/j.ijbiomac.2021.10.030

Santhi, D., Kalaikannan, A., & Sureshkumar, S. (2015). Factors influencing meat emulsion properties and product texture: A review. *Critical Reviews in Food Science and Nutrition, 57*(10), 2021–2027. https://doi.org/10.1080/10408398.2013.858027

Saygi, D., Ercoşkun, H., & Şahin, E. (2018). Hazelnut as functional food component and fat replacer in fermented sausage. *Journal of Food Science and Technology, 55*, 3385–3390. https://doi.org/10.1007/s13197-018-3129-7

Shi, Y., Li, J., Gu, L., Su, Y., Chen, W., Zhang, M., Chang, C., & Yang, Y. (2022). Synergistic effect of gum arabic and xanthan gum on improving rheological properties of low-fat mayonnaise with egg white protein microparticle as a fat mimetic. *International Journal of Food Science & Technology, 58*(3), 1037–1048. https://doi.org/10.1111/ijfs.16237

Sinthusamran, S., Benjakul, S., Swedlund, P. J., & Hemar, Y. (2017). Physical and rheological properties of fish gelatin gel as influenced by κ-carrageenan. *Food Bioscience, 20*, 88–95. https://doi.org/10.1016/j.fbio.2017.09.001

Sun, J., Mu, Y., Mohammed, O., Dong, S., & Xu, B. (2020). Effects of single-mode microwave heating and dextran conjugation on the structure and functionality of ovalbumin–dextran conjugates. *Food Research International, 137*. https://doi.org/10.1016/j.foodres.2020.109468

Sun, Y., Jin, H., Sun, H., & Sheng, L. (2020). A comprehensive identification of chicken egg white phosphoproteomics based on a novel digestion approach. *Journal of Agricultural and Food Chemistry, 68*(34), 9213–9222. https://doi.org/10.1021/acs.jafc.0c03174

Weng, W., & Zheng, W. (2015). Silver carp (hypophthalmichthys molitrix) surimi acid-induced gel extract characteristics: A comparison with heat-induced gel. *International Journal of Food Properties, 18*(4), 821–832. https://doi.org/10.1080/10942912.2013.864675

Wilson, P. B. (2017). Recent advances in avian egg science: A review. *Poultry Science, 96*(10), 3747–3754. https://doi.org/10.3382/ps/pex187

Wu, D., Guo, J., Wang, X., Yang, K., Wang, L., Ma, J., Zhou, Y., & Sun, W. (2021). The direct current magnetic field improved the water retention of low-salt myofibrillar protein gel under low-temperature conditions. *LWT - Food Science and Technology, 151*. https://doi.org/10.1016/j.lwt.2021.112034

Wu, D., Mei, S., Duan, R., Geng, F., Wu, W., Li, X., Cheng, L., & Wang, C. (2019). How black tea pigment theaflavin dyes chicken eggs: Binding affinity study of theaflavin with ovalbumin. *Food Chemistry, 303*. https://doi.org/10.1016/j.foodchem.2019.125407

Xia, M., Zhao, Q., Isobe, K., Handa, A., Cai, Z., & Huang, X. (2022). Lysozyme impacts gel properties of egg white protein via electrostatic interactions, polarity differences, local pH regulation, or as a filler. *International Journal of Biological Macromolecules, 223(B)*, 1727–1736. https://doi.org/10.1016/j.ijbiomac.2022.10.101

Xue, H., Tu, Y., Zhang, G., Xin, X., Hu, H., Qiu, W., Ruan, D., & Zhao, Y. (2021). Mechanism of ultrasound and tea polyphenol assisted ultrasound modification of egg white protein gel. *Ultrasonics Sonochemistry, 81*. https://doi.org/10.1016/j.ultsonch.2021.105857

Yang, S., Zhang, G., Chu, H., Du, P., Li, A., Liu, L., & Li, C. (2023). Changes in the functional properties of casein conjugates prepared by Maillard reaction with pectin or arabinogalactan. *Food Research International, 165*. https://doi.org/10.1016/j.foodres.2023.112510

Yang, X., Li, A., Li, X., Sun, L., & Guo, Y. (2020). An overview of classifications, properties of food polysaccharides and their links to applications in improving food textures. *Trends in Food Science & Technology, 102*, 1–15. https://doi.org/10.1016/j.tifs.2020.05.020

Yong, H., Ningning, W., Xiaoqiang, G., Tifeng, J., & Hao, D. (2021). Influence of ultrasound on the adsorption of single-walled carbon nanotubes to phenol: A study by molecular dynamics simulation and experiment. *Chemical Engineering Journal, 427*. https://doi.org/10.1016/j.cej.2021.131819

Yoshizawa, T., Shimizu, T., Yamabe, M., Taichi, M., Nishiuchi, Y., Shichijo, N., Unzai, S., Hirano, H., Sato, M., & Hashimoto, H. (2011). Crystal structure of basic 7S globulin, a xyloglucan-specific endo-β-1,4-glucanase inhibitor protein-like protein from soybean lacking inhibitory activity against endo-β-glucanase. *The FEBS Journal, 278*(11), 1944–1954. https://doi.org/10.1111/j.1742-4658.2011.08111.x

Yu, X.-X., Chi, S.-X., Wang, X.-H., Liu, B.-H., Wang, Y., & Zhang, Y.-H. (2023). Preparation of fat substitute based on maize starch hydrolysates and application in reduced-fat acidified milk gel. *International Journal of Biological Macromolecules, 244*. https://doi.org/10.1016/j.ijbiomac.2023.125479

Yuan, S., Chan, H. C. S., & Hu, Z. (2017). Using PyMOL as a platform for computational drug design. *Wiley Interdisciplinary Reviews: Computational Molecular Science, 7*(2), E1298. https://doi.org/10.1002/wcms.1298

Zaferani, S. P. G., Amiri, M. K., & Amooey, A. A. (2024). Computational AI to predict and optimize the relationship between dye removal efficiency and Gibbs free energy in the adsorption process utilizing TiO2/chitosan-polyacrylamide composite. *International Journal of Biological Macromolecules, 264*(2). https://doi.org/10.1016/j.ijbiomac.2024.130738

Zhang, K. Y., Liu, S., Liang, S. N., Xiang, F. Q., Wang, X. D., Lian, H. Q., … Liu, F. (2024). Exopolysaccharides of lactic acid bacteria: Structure, biological activity, structure-activity relationship, and application in the food industry: A review. *International Journal of Biological Macromolecules, 257*, Article 128733. https://doi.org/10.1016/j.foodchem.2024.138982

Zhang, M., Mei, L., Wu, Y., Jin, G., & Bao, D. (2023). Impact of ethanol extract of propolis on heat-induced egg white protein gels: Formation and properties. *Food Hydrocolloids, 149*. https://doi.org/10.1016/j.foodhyd.2023.109590

Zhang, X., Chen, G., Cai, L., Wang, Y., Sun, L., & Zhao, Y. (2021). Bioinspired pagoda-like microneedle patches with strong fixation and hemostasis capabilities. *Chemical Engineering Journal, 414*. https://doi.org/10.1016/j.cej.2021.128905

Zhang, Z., Yang, Y., Zhou, P., Zhang, X., & Wang, J. (2016). Effects of high pressure modification on conformation and gelation properties of myofibrillar protein. *Food Chemistry, 217*, 678–686. https://doi.org/10.1016/j.foodchem.2016.09.040

Zhao, X., Guo, R., Li, X., Wang, X., Zeng, L., Wen, X., & Huang, Q. (2022). Effect of oil-modified crosslinked starch as a new fat replacer on gel properties, water distribution, and microstructures of pork meat batter. *Food Chemistry, 409*. https://doi.org/10.1016/j.foodchem.2022.135337

Zhao, X., Zhuang, H., Yoon, S.-C., Dong, Y., Wang, W., & Zhao, W. (2017). Electrical impedance spectroscopy for quality assessment of meat and fish: A review on basic principles, measurement methods, and recent advances. *Journal of Food Quality, 2017*(1). https://doi.org/10.1155/2017/6370739

Zhou, Y., Cui, Y., & Qu, X. (2018). Exopolysaccharides of lactic acid bacteria: Structure, bioactivity and associations: A review. *Carbohydrate Polymers, 207*, 317–332. https://doi.org/10.1016/j.carbpol.2018.11.093

Zhu, J., Wang, C., Gao, J., Wu, H., & Sun, Q. (2019). Aggregation of fucoxanthin and its effects on binding and delivery properties of whey proteins. *Journal of Agricultural and Food Chemistry, 67*(37), 10412–10422. https://doi.org/10.1021/acs.jafc.9b03046